Ultra-thin film sensors based on porphyrin-5-ylphosphonate diesters for selective and sensitive dual-channel optical detection of mercury(II) ions

Alla G. Bessmertnykh-Lemeune, Elizaveta V Ermakova, Elena O Koroleva, Alexander V Shokurov, Vladimir V Arslanov, Alla Bessmertnykh-Lemeune

Ultra-thin film sensors based on porphyrin-5-ylphosphonate diesters for selective and sensitive dual-channel optical detection of mercury(II) ions

Elizaveta V. Ermakova,[†] Elena O. Koroleva,[†] Alexander V. Shokurov,[†] Vladimir V. Arslanov*[†] and Alla Bessmertnykh-Lemeune*[‡,§]*

[†] Frumkin Institute of Physical Chemistry and Electrochemistry, Russian Academy of Sciences, Leninsky Pr. 31-4, Moscow 119071, Russia

[‡] Institut de Chimie Moléculaire de l'Université de Bourgogne, Université Bourgogne Franche-Comté, CNRS UMR 6302, 9 Avenue Alain Savary, BP 47870, Dijon 21078 CEDEX, France

[§] ENS de Lyon, CNRS UMR 5182, Université Claude Bernard Lyon 1, Laboratoire de Chimie, F69342, Lyon, France

Corresponding Authors

*E-mail: evermakova92@gmail.com (Elizaveta V. Ermakova), vladimir.arslanov@gmail.com (Vladimir V. Arslanov), alla.lemeune@ens-lyon.fr (Alla Bessmertnykh-Lemeune)

KEYWORDS: porphyrin, solid thin-film sensor, mercury(II) detection, Langmuir monolayer, Langmuir-Schaefer film, dual-channel optical sensor

ABSTRACT

Reusable dual-channel optical sensors for Hg^{2+} ions were prepared by Langmuir-Schaefer (LS) method from amphiphilic (*trans*-A_2)BC-type porphyrins functionalized at *meso*-positions of the tetrapyrrolic macrocycle by sterically demanding diethoxyphosphoryl and mesityl groups as well as electron donating RO, RS or RNH substituents (R = *n*-C_8H_{17}). These three novel amphiphilic

porphyrin derivatives were synthesized in good yields and their floating films at the air–water interface were investigated. In these monolayers, porphyrin molecules display a slipped stack-of-card orientation, but their strong π stacking is prohibited by bulky diethoxyphosphoryl and mesityl groups. The heteroatom substituent plays a key role in the molecular organization of the monolayers because it can participate in intermolecular hydrogen bonding, which influences the monolayer structure. Sensing properties of the porphyrins organized in Langmuir monolayers differ from those in the solution environment. Selective spectrophotometric detection of Hg^{2+} ions by these floating films is observed because interfering Cu^{2+}, Zn^{2+}, Cd^{2+}, and Pb^{2+} ions are coordinated to donor centers located at the periphery of the macrocycle. Transfer of these floating films onto a polyvinyl chloride surface by LS technique affords perforated multilayer films with a tight molecular coverage of the solid support. The effect of the heteroatoms on the organization of these films was demonstrated by scanning electron microscopy (SEM) and electrochemical impedance spectroscopy (EIS). Both absorption and emission studies provide a strong evidence that chromophore-chromophore interactions are rather weak in these LS films. Binding of mercury(II) ions by the films and the regeneration of the sensors were explored visually and using reflection absorbance and fluorescence spectroscopies and then confirmed by X-ray fluorescence analysis. Detection limit of these selective and reusable dual-channel (absorbance and fluorescence) thin-film sensors is about 10^{-8} M (2 ppb), that corresponds to the action level for Hg^{2+} ions in drinking water recommended by the U.S. Environmental Protection Agency (EPA).

1. Introduction

Reusable, sensitive and selective optical sensors for mercury(II) ions are constantly required due to the increase of metal contamination in environment and toxic effects of this

pollutant on living matter [1-4]. The mercury content in fish, human hair, and other biological specimens around the world is regularly reported to exceed the permitted level. The prolonged exposure of humans to even very low concentrations of Hg^{2+} can lead to neurological diseases, various cognitive and motion disorders, damage to the prenatal brain, digestive system and kidneys. Mercury is one of the most toxic metals and the maximal level established by the US Environment Protection Agency (EPA) for the content of this ion in drinking water is as low as 2 ppb (0.01 μM) [5]. Common organic chemosensors, in which the signal transduction is achieved through changing light absorption and/or emission, are cost-efficient and useful for real-time and place analysis of environmental and biomedical samples. However, they commonly exhibit a high limit of detection (LOD), which is a serious drawback for their usefulness in the analysis of Hg^{2+} in aqueous samples. From this standpoint, the key goal in the development of such systems is the enhancement of their sensitivity to the analyte.

Porphyrins have been widely applied for the development of sensors due to their compatibility with a wide range of transduction mechanisms and numerous pathways of their interactions with target analytes (spanning from the weak Van der Waals forces to π-interactions, hydrogen bonding, and coordination to the central metal ion of metalloporphyrins or chelation of metal ions by free base porphyrins) [6-8]. In particular, their light absorption and emission properties are suitable for fabrication of highly sensitive optical sensors due to their remarkable molar extinction and attractive luminescence quantum yields (about 10%) [8-13]. Moreover, experimental research has shown that porphyrins offer fascinating sensing opportunities, since they combine a high reactivity and the possibility of tuning their sensing properties by choosing appropriate metals at the

center of the tetrapyrrolic ring and the peripheral substituents. More recently, supramolecular chemistry concepts further enriched the value of porphyrin sensors [14], while well-developed synthetic chemistry has rendered them suitable to surface functionalization, expanding their attractiveness for preparation of sensory devices [15].

Free base porphyrins were widely explored for the detection of toxic metal ions, including mercury(II) ions, because the coordination of metal ions to pyrrolic nitrogen atoms can be easily detected by optical spectroscopy or even visually [16-22]. However, these chelators coordinate many soft metal ions and exhibit a low selectivity. These ligands, like the vast majority of chemosensors, are insoluble in water and the synthesis of their hydrophilic derivatives is somewhat laborious. Moreover, in aqueous media, the rate of the complex formation and fluorescence quantum yields could be reduced in part due to the tendency of planar and highly polarizable porphyrin molecules to aggregate under these conditions. All these limitations significantly complicate the use of porphyrins in the preparation of sensory systems.

To overcome these drawbacks, several approaches were developed. Cyclodextrin–porphyrin inclusion complexes have been proposed as sensory systems to increase the water solubility of the sensor molecules [23-25]. Another strategy is a conjugation of the porphyrin with a hydrophilic ionophore [26-32]. In these modular molecules, metalloporphyrin fragment serves only as a signaling unit and is separated from the receptor unit by a phenylene or longer spacer. Commonly, addition of metal ions induces only very small changes in the absorption spectra of these compounds. Therefore, recent investigations were focused on the preparation of solid-state sensors based on free base porphyrins, such as sensory sol-gel bulk materials and thin films [33-37],

porphyrin–polymer films [17, 38-41], or membranes [42-45], porphyrin-functionalized nanoparticles [46-49], porphyrin-modified fibers [50], porphyrin–graphene oxide nanocomposites [51], porphyrin-containing MOFs [52], porphyrin chemosensors grafted on mesoporous silica [53], self-assembled films and aggregates [6, 54-56]. These molecular materials are technologically attractive due to their potential ease of use. Moreover, several of them demonstrate a high selectivity to Hg^{2+} ions that likely can be explained by a competitive complexation of interfering metal ions by the solid support [42, 43, 45, 48, 50, 51, 57]. Some of these systems can be used as dual-channel (light absorption and emission) sensors as summarized in Table S1.

One of promising approaches to solid-state sensors, which can solve many of problems in question, is the immobilization of water-insoluble porphyrins onto solid supports through the preparation of Langmuir monolayers followed by their assembling into Langmuir-Blodgett (LB) or Langmuir-Schaefer (LS) films [58-63]. This strategy has been widely investigated for the fabrication of highly ordered ultra-thin films by virtue of its general applicability for controlling the molecular orientation in the films. Langmuir monolayer method and LB/LS techniques allow one not only to study and finely control the process of molecular organization at the stage of the monolayer assembly, but also to gain a deeper insight into molecular recognition, receptor and sensory phenomena that occur in the porphyrin-based self-assembled systems on surfaces.

Furthermore, LB and LS film thickness may be precisely controlled, which is important for achieving high sensitivity of ultra-thin sensory films. Finally, both fabrication of sensors and analytical tests may be performed in an aqueous medium using a minimum amount of organic solvents and expensive porphyrins if the experimental conditions for a quantitative transfer of floating films onto a solid support are found.

The LB and LS films formed by free base porphyrins and their complexes at air–water and air–solid interfaces hold promise for different technical applications such as nonlinear optics, electronics, solar cell development, catalysis and pharmacology [64-74]. The influence of metal ions and peripheral substituents on the organization of porphyrin supramolecular assemblies at the air–water interface and their transfer onto solid supports have been thoroughly investigated [75-80]. The ultra-thin films prepared by these methods were also widely used for detection of gases or volatile organic compounds (VOCs) in gaseous phase [72, 79, 81-86]. It is somewhat surprising however, that this great effort devoted to the preparation of sensing monolayers has generated only a few examples of porphyrin-based sensors operating in aqueous solutions [87]. The sensory systems, which are stable in aqueous media and suitable for detection of Hg^{2+} ions, were reported only recently [88, 89]. They were prepared from commercially available 5,10,15,20-tetraphenyl- (**TPP**) [88] and 5,10,15,20-tetra(4-pyridyl)porphyrins (**TPyP**) [89] and only the latter is relevant to optical methods. Using this film, Hg^{2+} and Cu^{2+} ions can be distinguished in aqueous solutions.

According to investigations of porphyrin LB and LS films, the sensing porphyrin monolayers are usually formed by molecules self-assembled through strong π–π stacking. The supramolecular interactions influence the absorption and emission properties of porphyrin molecules and their ability to bind the target analyte [14, 90-92]. To circumvent these problems, it would be useful to prepare porphyrin derivatives that are amenable to the formation of ordered films yet isolate the chromophore molecules minimizing the electronic interactions of adjacent molecules.

Recently, we reported a novel family of (*trans*-A_2)BC-type porphyrins (A = Ph) bearing a bulky and hydrophilic diethoxyphosphoryl substituent and RS, RO or RNH groups with a rather long alkyl chain (R = *n*-C_8H_{17}) at opposite *meso*-positions of the macrocycle (two RO-substituted

derivatives **DPOP** and **DPOPhP** are depicted in Fig. 1) [93]. These compounds being amphiphilic may allow for the formation of the Langmuir monolayers at air–water interfaces [64, 69, 75, 91]. Moreover, the electron donating character of the heteroatom substituent is adequate to enhance the Hg^{2+} coordination by the macrocycle [57].

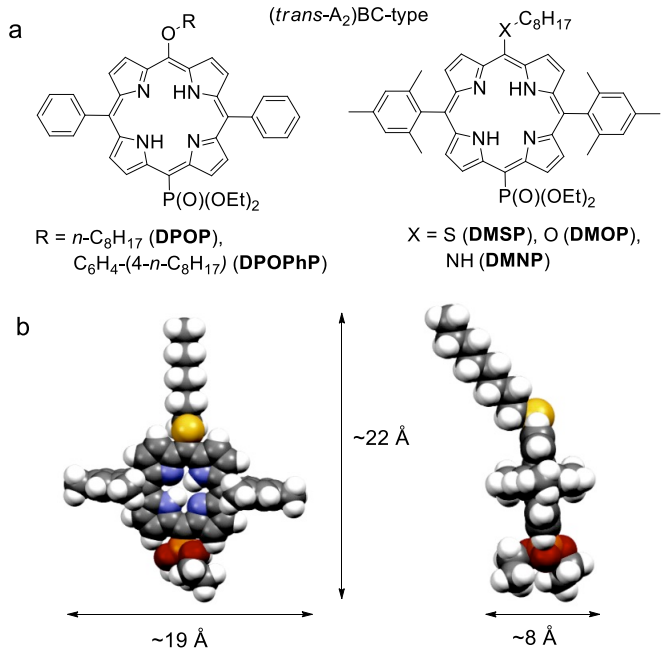

Fig. 1. (a) Structures of porphyrinylphosphonate diesters referenced (**DPOP** and **DPOPhP**) and investigated in this study (**DMOP**, **DMSP** and **DMNP**). (b) Spacefill model of **DMSP** molecule optimized by the semi-empirical PM6 method [94].

Indeed, porphyrins **DPOP** and **DPOPhP** form rarefied films on liquid and solid surfaces, in which electronic interactions of adjacent porphyrin molecules are either weak or altogether absent [93]. The bulky diethyl phosphonate group (Fig. 1) seems to prevent the formation of tightly packed porphyrin aggregates, while the substituent containing the alkyl chain and the phosphonate group determine a preferential orientation of the molecules in the studied monolayers. Moreover, in the LS films, these two oppositely located substituents serve as an efficient spacer of porphyrin

macrocycles belonging to adjacent layers. This allowed us to prepare emissive LS films of the free base porphyrins **DPOP** and **DPOPhP** on the polyvinyl chloride (PVC) surface. The sensing properties of these films have not been explored up to now. However, our preliminary investigation has shown that the monolayers formed by **DPOP** at the air–water interface can coordinate zinc(II) ions [93].

In this work, solid-state sensors for mercury(II) ions were prepared from porphyrinylphosphonate diesters **DMOP**, **DMSP** and **DMNP** by LS technique (Fig. 1). To this end, we optimized the structural parameters of porphyrinylphosphonate diesters replacing two phenyl substituents at the porphyrin skeleton by sterically demanding hydrophobic mesityl groups. This structural modification should stabilize the porphyrin monolayers and decrease leaching of amphiphilic porphyrin molecules into aqueous solution during the analysis and regeneration of the sensor. Three *meso*-heteroatom-substituted derivatives differed only in the nature of the peripheral donor site XR (X = NH, O, S) were prepared to evaluate the influence of this site on the structure of self-assembled films and the selectivity of Hg^{2+} detection. As a result of these systematic studies, we developed sensitive, reusable, and cost-efficient solid sensors for detection of mercury(II) ions, which is useful for the analysis of environmental samples and drinking water. In contrast to previously reported sensory LS films, these materials allow for the selective dual-channel (colorimetric and fluorescence) detection of Hg^{2+} ions due to coordination of interfering metal ions to the donor heteroatoms located at the periphery of the porphyrin macrocycle.

2. Experimental Section

2.1 General considerations. Unless otherwise noted, all chemicals and starting materials were obtained commercially from Acros® or Aldrich® and used without further purification. DMA was dried with molecular sieves. Cs_2CO_3 was dried under reduced pressure at 120 °C for 48 h.

Chloroform (analytical grade) and methanol (99.8%) were purchased from Merck. All metal salts used were perchlorates of general $M(ClO_4)_n \cdot xH_2O$ formula. *Caution! Although no problems were experienced, perchlorate salts are potentially explosive when combined with organic ligands and should be manipulated with care and used only in very small quantities.*

5,15-Dimesitylporphyrin and (5,15-Dimesitylporphyrinato)zinc (**1a**) were prepared according to published procedures [95]. [10-(Diethoxyphosphoryl)-5,15-diphenylporphyrinato]zinc (**2a**) was obtained in 52 % yield according to a two-steps procedure involving bromination of porphyrin **1a** (1.3 g, 2.13 mmol) followed by Pd-catalyzed phosphonilation [63].

^{1}H and ^{31}P NMR spectra were acquired either on a Bruker Avance III Nanobay 300 MHz and a Bruker Avance III 600 MHz spectrometers. Chemical shifts are expressed in parts per million (ppm), referenced on the δ scale by using residual non-deuterated solvent signals as internal standard for ^{1}H NMR spectroscopy and external phosphonic acid (H_3PO_4) for ^{31}P NMR spectroscopy. The coupling constants are expressed in units of frequency (Hz). Accurate mass measurements (HRMS) were made on a THERMO LTQ Orbitrap XL equipped with an electrospray ionisation (ESI) source in positive mode unless otherwise stated. Solutions in $CHCl_3$/methanol (1:1) were used for the analysis. IR spectra were registered on Bruker Vector 22 spectrophotometer. Universal micro-ATR sampling accessory (Pike) was used in order to obtain IR spectra of solid samples. UV-visible absorption spectra were obtained on a Varian Cary 50 spectrophotometer by using a rectangular quartz cell (Hellma, 100-QS, 45 × 12.5 × 12.5 mm, pathlength: 10 mm, chamber volume: 3.5 mL). MALDI-TOF mass-spectra were obtained on a Bruker Ultraflex II LRF 2000 mass-spectrometer in positive ion mode with dithranol matrix. Analytical thin-layer chromatography (TLC) was carried out using Merck silica gel 60 F-254 plates (precoated sheets, 0.2 mm thick, with fluorescence indicator F254).

All the spectrometers were available at the "Pôle Chimie Moléculaire", the technological platform for chemical analysis and molecular synthesis (http://www.wpcm.fr) which relies on the Institute of the Molecular Chemistry of University of Burgundy and WelienceTM, a Burgundy University private subsidiary.

2.2 Synthesis of porphyrins

[5-Bromo-15-(diethoxyphosphoryl)-10,20-dimesitylporphyrinato(2-)]zinc (3a). To a solution of porphyrin **2a** (300 mg, 0.40 mmol) in chloroform (100 mL), pyridine (310 μL, 3.78 mmol) was added and the solution was stirred for 10 min at room temperature. The reaction mixture was cooled to –7 °C and then NBS (78 mg, 0.44 mmol) was added in one portion. The reaction was quenched after 10 min by the addition of acetone (10 mL). Then the reaction mixture was evaporated under reduced pressure and the crude solid residue was purified by column chromatography using CH_2Cl_2/MeOH (gradient elution, 0–0.4 v/v % of MeOH) as an eluent. Fractions containing the target product were identified by TLC, combined, evaporated under reduced pressure and dried overnight (2 mm Hg) to afford **3a** as a dark violet solid in 90% yield (297 mg). ^{1}H NMR (300 MHz, $CDCl_3$/CD_3OD 2:1, v/v, 25°C): δ_H = 9.85 (dd, $^3J_{H,H}$ = 4.6 Hz, $^3J_{P,H}$ = 0.7 Hz, 2H, *β*-H), 9.36 (d, $^3J_{H,H}$ = 4.6 Hz, 2H, *β*-H), 8.46 (br d, $^3J_{H,H}$ = 4.9 Hz, 2H, *β*-H), 8.40 (d, $^3J_{H,H}$ = 4.6 Hz, 2H, *β*-H), 7.06 (br s, 4H, Mes), 4.20–4.34 (m, 2H, $POCH_2$), 3.96–4.10 (m, 2H, $POCH_2$), 2.43 (s, 6H, *p*-Me), 1.65 (s, 12H, *o*-Me), 1.15 (t, $^3J_{H,H}$ = 7.0 Hz, 6H, $OCH_2\underline{Me}$) ppm. $^{31}P\{^1H\}$ NMR (121 MHz, $CDCl_3$/CD_3OD, 2:1 v/v, 25°C) : δ_P (ppm) 26.45 ppm. HRMS (ESI): *m/z* calcd. for $C_{42}H_{41}BrN_4O_3PZn$ $[M+H]^+$ 823.13856, found 823.13778; calcd. for $C_{42}H_{40}BrN_4O_3PZnNa$ $[M+Na]^+$ 845.12051, found 845.11881. FT-IR (neat): ν_{max} 2976 (m), 2960 (m), 2921 (m), 1548 (m), 1467 (m), 1436 (m), 1391 (w), 1377 (w), 1355 (w), 1320 (m), 1287 (w), 1216 (s, P=O), 1199 (s), 1161 (w), 1085 (m), 1069 (m), 1044 (m), 1016 (s), 1000 (s, P–O), 983 (s,

P–O), 965 (m), 885 (s), 855 (s), 789 (c), 757 (s), 596 (m), 561 (m), 536 (m) cm^{-1}. UV-Vis ($CHCl_3$): λ_{max} [log ε (M^{-1} cm^{-1})] = 324 (4.27), 427 (5.53), 555 (4.15), 590 (4.09), 606 nm (3.89).

[5-(Diethoxyphosphoryl)-15-(octyloxy)-10,20-dimesitylporphyrinato]zinc (ZnDMOP). A 10 mL two-necked flask equipped with a magnetic stirrer and a back-flow condenser was charged with porphyrin **3a** (33 mg, 0.04 mmol) and cesium carbonate (130.0 mg, 0.40 mmol). The reaction vessel was evacuated and purged by N_2 for 3 times. Subsequently, 4.5 mL of 1-octanol was added by syringe and the mixture was stirred at 85 °C for 4 h. After cooling, the reaction mixture was evaporated under reduced pressure. The residue was purified by column chromatography on silica gel using CH_2Cl_2 and CH_2Cl_2/MeOH (99:1, v/v) as eluents. The target compound **ZnDMOP** was isolated as a violet solid in 52% yield (18 mg). ^{1}H NMR (600 MHz, $CDCl_3$/CD_3OD 2:1, v/v, 25°C): δ_H = 9.97 (br d, $^3J_{H,H}$ = 5.0 Hz, 2H, β-H), 9.35 (d, $^3J_{H,H}$ = 4.6 Hz, 2H, β-H), 8.63 (d, $^3J_{H,H}$ = 5.0 Hz, 2H, β-H), 8.53 (d, $^3J_{H,H}$ = 4.6 Hz, 2H, β-H), 7.27 (br s, 4H, Mes), 5.07 (t, $^3J_{H,H}$ = 7.1 Hz, 2H, $OC\underline{H}_2C_7H_{15}$), 4.48–4.46 (m, 2H, $POCH_2$), 4.26–4.18 (m, 2H, $POCH_2$), 2.63 (s, 6H, *p*-Me), 2.38–2.36 (m, 2H, $OCH_2C\underline{H}_2C_6H_{13}$), 1.93–1.87 (m, 2H, $OC_2H_4C\underline{H}_2C_5H_{11}$), 1.84 (s, 12H, *o*-Me), 1.61–1.55 (m, 2H, $OC_3H_6C\underline{H}_2C_4H_9$), 1.50–1.44 (m, 2H, $OC_4H_8C\underline{H}_2C_3H_7$), 1.38–1.37 (m, 4H, $OC_5H_{10}(C\underline{H}_2)_2Me$), 1.35 (t, $^3J_{H,H}$ = 7.1 Hz, 6H, $OCH_2\underline{Me}$), 0.92 (t, $^3J_{H,H}$ = 7.1 Hz, 3H, $OC_7H_{14}\underline{Me}$) ppm. $^{31}P\{^1H\}$ NMR (243 MHz, $CDCl_3$/CD_3OD 2:1, v/v, 25 °C): δ_P = 27.37 ppm. FT-IR (neat): ν_{max} = 3232 (w), 2925 (m), 2855 (m), 2362 (m), 2052 (w), 1916 (w), 1899 (w), 1879 (w), 1792 (w), 1770 (w), 1734 (w), 1683 (w), 1652 (w), 1611 (w), 1549 (m), 1531 (w), 1464 (m), 1440 (m), 1391 (w), 1378 (w), 1355 (m), 1322 (m), 1287 (m), 1263 (m), 1218 (m, P=O), 1201 (s, P=O), 1158 (m), 1085 (m), 1060 (m), 1047 (m), 1013 (s), 983 (s, P–O), 886 (s), 852 (m), 824 (m), 797 (s), 764 (m), 749 (m), 730 (m),

718 (m), 702 (m), 672 (w), 663 (w), 629 (w), 596 (m), 673 (m), 563 (m), 537 (m), 517 (w) cm^{-1}. UV-Vis ($CHCl_3$/MeOH 2:1, v/v): λ_{max} [log ε (M^{-1} cm^{-1})] = 403 (4.57), 422 (5.37), 517 (3.48), 556 (4.10), 587 (3.67), 600 nm (3.64). MS (MALDI-TOF): *m*/*z* calcd. for $C_{50}H_{58}N_4O_4PZn$ $[M + H]^+$ 873.35; found 873.56.

Diethyl [15-(octyloxy)-10,20-dimesitylporphyrin-5-yl]phosphonate (DMOP). A 100 mL two-necked flask equipped with a magnetic stirrer and a back-flow condenser was charged with **ZnDMOP** (18 mg, 0.022 mmol). Subsequently, 75.0 mL of chloroform and 200 µL of HCl were added by syringe and the mixture was stirred at room temperature for 1 h. Then the mixture was washed with distilled water (4 x 25 mL). The organic phase was dried over $MgSO_4$, filtered and evaporated under reduced pressure. The target compound **DMOP** was isolated as a red solid in 95% yield (17 mg). UV/Vis ($CHCl_3$): λ_{max} [log ε (M^{-1} cm^{-1})] = 370 (4.18), 418 (5.10), 490 (3.85), 517 (4.24), 551 (3.89), 587 (3.79), 640 nm (3.41). The purity of compound was checked by thin-layer chromatography and MALDI-TOF analysis. MS (MALDI-TOF): *m*/*z* calcd. for $C_{50}H_{61}N_4O_4P[M+H]^+$ 811.44, found 811.68.

[5-(Diethoxyphosphoryl)-15-(octylsulfanyl)-10,20-dimesitylporphyrinato]zinc (ZnDMSP). A 10 mL two-necked flask equipped with a magnetic stirrer and a back-flow condenser was charged with porphyrin **3a** (30 mg, 0.036 mmol) and cesium carbonate (119 mg, 0.36 mmol). The reaction vessel was evacuated and purged by N_2 for 3 times. Subsequently, 4.4 mL of 1-octanethiol was added by syringe and the mixture was stirred at room temperature for 2 h. After that, the mixture was evaporated under reduced pressure. The residue was purified by column chromatography on silica gel using CH_2Cl_2 and CH_2Cl_2/MeOH (90:10, v/v) as eluents. The target compound **ZnDMSP** was isolated as a violet solid in 68% yield (22 mg).

^{1}H NMR (600 MHz, $CDCl_3/CD_3OD$ 2:1, v/v, 25°C): δ_H = 10.11 (br d, $^{3}J_{H,H}$ = 5.0 Hz, 2H, β-H), 9.92 (d, $^{3}J_{H,H}$ = 4.6 Hz, 2H, β-H), 8.71 (d, $^{3}J_{H,H}$ = 5.0 Hz, 2H, β-H), 8.66 (d, $^{3}J_{H,H}$ = 5.0 Hz, 2H, β-H), 7.29 (s, 4H, Mes), 4.48–4.43 (m, 2H, OCH_2), 4.25–4.20 (m, 2H, OCH_2), 3.45 (t, $^{3}J_{H,H}$ = 7.0 Hz, 2H, $SC\underline{H}_2$), 2.63 (s, 6H, *p*-Me), 1.83 (s, 12H, *o*-Me), 1.60–1.55 (m, 2H, $SCH_2C\underline{H}_2$), 1.42–1.38 (m, 2H, $S(CH_2)_2C\underline{H}_2$), 1.35 (t, $^{3}J_{H,H}$ = 7.1 Hz, 6H, $OCH_2\underline{Me}$), 1.11–1.03 (m, 8H, $S(CH_2)_3(C\underline{H}_2)_4$), 0.73 (t, $^{3}J_{H,H}$ = 7.1 Hz, 3H, Me) ppm. $^{31}P\{^{1}H\}$ NMR (243 MHz, $CDCl_3/CD_3OD$ 2:1, v/v, 25 °C): δ_P = 26.41 ppm. FT-IR (neat): ν_{max} = 2922 (m), 2853 (m), 2778 (w), 2731 (w), 2528 (w), 2356 (w), 2325 (w), 2289 (w), 2243 (w), 2165 (w), 2145 (w), 2111 (w), 2071 (w), 2052 (w), 2011 (w), 1982 (w), 1967 (w), 1950 (w), 1916 (w), 1885 (w), 1810 (w), 1779 (w), 1713 (w), 1661 (w), 1633 (w), 1612 (w), 1568 (w), 1549 (w), 1519 (w), 1455 (m), 1435 (m), 1412 (m), 1391 (m), 1377 (m), 1354 (w), 1318 (w), 1288 (w), 1265 (w), 1213 (m, P=O), 1195 (m, P=O), 1160 (m), 1085 (m), 1062 (w), 1045 (m), 1015 (s), 982 (s, P–O), 961 (s, P–O), 885 (m), 850 (s), 829 (m), 795 (s), 745 (m), 723 (m), 714 (m), 681 (w), 670 (w), 649 (m), 596 (m), 580 (m), 561 (m), 535 (m), 510 (m) cm^{-1}. UV-Vis ($CHCl_3$/MeOH 2:1, v/v): λ_{max} [log ε (M^{-1} cm^{-1})] = 329 (4.14), 405 (4.59), 427 (5.38), 525 (3.40), 561 (3.96), 595 (4.11), 611 nm (3.90). MS (MALDI-TOF): *m*/*z* calcd. for $C_{50}H_{58}N_4O_3SPZn$ $[M + H]^+$ 889.33; found 889.47.

Diethyl [15-4-(octylsulfanyl)-10,20-dimesitylporphyrin-5-yl]phosphonate (DMSP). A 100 mL two-necked flask equipped with a magnetic stirrer and a back-flow condenser was charged with **ZnDMSP** (22 mg, 0.024 mmol). Subsequently, 50.0 mL of chloroform and 150 µL of HCl were added by syringe and the mixture was stirred at room temperature for 1 h. Then the mixture was washed with distilled water (4x20 mL). The organic phase was dried over $MgSO_4$, filtered and evaporated under reduced pressure. The target

compound **DMSP** was isolated as a red solid in 94% yield (19.0 mg). UV-Vis ($CHCl_3$): λ_{max} [log ε (M^{-1} cm^{-1})] = 370 (4.42), 421 (5.16), 490 (3.62), 520 (4.09), 558 (4.03), 595 (3.72), 650 nm (3.83). The purity of compound was checked by thin-layer chromatography and MALDI-TOF analysis. MS (MALDI-TOF): *m*/*z* calcd. for $C_{50}H_{60}N_4O_3SP$ $[M + H]^+$ 827.41; found 827.78.

[5-(Diethoxyphosphoryl)-15-(octylamino)-10,20-diphenylporphyrinato]zinc (ZnDMNP). A 10 mL two-necked flask equipped with a magnetic stirrer and a back-flow condenser was charged with porphyrin **3a** (30 mg, 0.036 mmol), palladium acetate (0.4 mg, 0.002 mmol), BINAP (1.9 mg, 0.003 mmol) and cesium carbonate (17 mg, 0.05 mmol). The reaction vessel was evacuated and purged by N_2 for 3 times. Subsequently, 4 mL of anhydrous toluene was added by syringe. After that, octylamine (60 μL, 0.36 mmol) was added by syringe and the mixture was stirred at reflux for 19 h. After cooling, the reaction mixture was evaporated under reduced pressure. The residue was purified by column chromatography on silica gel using $CHCl_3$/pentane (2:3, v/v) as eluent. The target compound **ZnDMNP** was isolated as a green-violet solid in 64% yield (20 mg). ^{1}H NMR (600 MHz, $CDCl_3/CD_3OD$ 2:1, v/v, 25 °C): δ_H = 9.33 (br d, $^3J_{H,H}$ = 4.9 Hz, 2H, β-H), 8.78 (d, $^3J_{H,H}$ = 4.4 Hz, 2H, β-H), 8.11 (d, $^3J_{H,H}$ = 4.9 Hz, 2H, β-H), 7.95 (d, $^3J_{H,H}$ = 4.4 Hz, 2H, β-H), 7.12 (s, 4H, Mes), 4.31−4.27 (m, 2H, $POCH_2$), 4.24 (t, $^3J_{H,H}$ = 7.2 Hz, 2H, $NC\underline{H}_2$), 4.11−4.07 (m, 2H, $POCH_2$), 4.00 (br t, 1H, NH), 2.49 (s, 6H, *p*-Me), 1.80 (s, 12H, *o*-Me), 1.54−1.48 (m, 2H, CH_2), 1.34−1.29 (m, 2H, CH_2), 1.26 (t, $^3J_{H,H}$ = 7.1 Hz, 6H, $OCH_2\underline{Me}$), 1.20−1.17 (m, 8H, CH_2), 0.77 (t, 3H, $^3J_{H,H}$ = 7.1 Hz, Me) ppm. $^{31}P\{^1H\}$NMR (600 MHz, $CDCl_3/CD_3OD$ 2:1, v/v, 25 °C): δ_P = 28.60 ppm. FT-IR (neat): ν_{max} = 3384 (w), 3374 (w), 3308 (w), 3261 (w), 3244 (w), 3228 (w), 3187 (w), 3143 (w), 3128 (w), 3098 (w), 3084

(w), 2955 (m), 2924 (m), 2855 (m), 2733 (w), 2538 (w), 2461 (w), 2361 (w), 2325 (w), 2225 (w), 2196 (w), 2167 (w), 2109 (w), 2075 (w), 2052 (w), 2044 (w), 2012 (w), 1998 (w), 1984 (w), 1882 (w), 1735 (w), 1611 (w), 1551 (m), 1503 (m), 1459 (m), 1377 (m), 1343 (m), 1320 (m), 1308 (m), 1271 (m, P=O), 1200 (m, P=O), 1160 (m), 1084 (m), 1050 (m), 1017 (s), 980 (m, P–O), 964 (m, P–O), 885 (m), 852 (m), 844 (m), 789 (m), 730 (m), 716 (m), 668 (w), 631 (m), 597 (m), 563 (m), 536 (m) cm^{-1}. UV-Vis ($CHCl_3$/MeOH 2:1, v/v): λ_{max} [log ε (M^{-1} cm^{-1})] = 330 (4.28), 403 (4.52), 424 (5.16), 440 (4.86), 515 (3.90), 552 (4.18), 590 (3.84), 606 nm (3.91). MS (MALDI-TOF): *m*/*z* calcd. for $C_{50}H_{59}N_5O_3PZn$ $[M + H]^+$ 872.36; found 872.49.

Diethyl [15-4-(octylamino)-10,20-dimesitylporphyrin-5-yl]phosphonate (DMNP). A 100 mL two-necked flask equipped with a magnetic stirrer and a back-flow condenser was charged with **ZnDMNP** (20 mg, 0.022 mmol). Subsequently, 50.0 mL of chloroform and 150 μL of HCl were added by syringe and the mixture was stirred at room temperature for 1 hours. Then the mixture was washed with distilled water (4 x 25 mL). The organic phase was dried over $MgSO_4$, filtered and evaporated under reduced pressure. The target compound **DMNP** was isolated as a red solid in 96% yield (17 mg). UV-Vis ($CHCl_3$): λ_{max} [log ε (M^{-1} cm^{-1})] = 421 (5.20), 437 (5.14), 507 (4.28), 548 (4.09), 582 (4.08), 656 nm (4.22). The purity of compound was checked by thin-layer chromatography and MALDI-TOF analysis. MS (MALDI-TOF): *m*/*z* calcd. for $C_{50}H_{61}N_5O_3P$ $[M + H]^+$ 810.44; found 810.28.

2.3 Visual detection of metal ions

The sensing properties of **DMSP**, **DMOP** and **DMNP** in the presence of metal ions were evaluated visually by adding gradually up to 1-3 equiv. of a 0.02 M methanol solution of metal perchlorate to **DMSP**, **DMOP** and **DMNP** (*c* = 0.05 mM) dissolved in chloroform.

Quenching of the solution fluorescence after addition of metal ions can be visually observed upon diode (λ = 365 nm) irradiation.

2.4 UV–vis absorption and fluorescent measurements of solutions and LS films

The UV–vis absorption spectra of solutions and LS films deposited onto solid substrates were recorded on a SHIMADZU-2450 spectrometer (Japan) in a wavelength range of 200-900 nm. The fluorescent spectra of solutions and LS films deposited onto solid substrates were recorded on a «SHIMADZU RF-5301» spectrofluorometer (Japan) in a wavelength range of 200-900 nm. The solution measurements were performed in a quartz cuvette with an optical path length of 1 cm at 20±1 ºC. Excitation wavelength of the porphyrins was 420 nm.

2.5 Preparation of Monolayers and LS films

A 1000-2 KSV Minitrough ($l \times w$ = 36.4 × 7.5 cm) model (KSV Instrument Ltd., Helsinki, Finland) equipped with a platinum Wilhelmy plate was used for preparation of Langmuir monolayers. The trough and barriers are made of Teflon. Monolayers were formed by spreading a freshly prepared 0.05 mM solutions of the ligands in chloroform. The deposited volume for spreading at the air–water interface was usually 200 μL. The spreading solution was deposited by means of a Gilson "Distriman" micropipette in 2.5 μL portions. Delivered drops were uniformly distributed over the available surface of water or aqueous solutions of perchlorate salts (1 mM). Deionized water (18.2 MΩ cm, pH ~5.5) produced by a Vodoley cartridge purificator (SPE Himelektronika, Russia) was used as a subphase.

After the sample has been spread, the solvent was allowed to evaporate for 15 min. All measurements were carried out at room temperature (20 ± 1 °C). The monolayer was compressed at a rate of 5 mm min^{-1}. Each compression isotherm was recorded at least three

times to ensure the reproducibility of the results. The sensitivity of the Wilhelmy plate method for surface pressure–area (π–A) isotherms was ±0.01 mN m^{-1}.

LS films were deposited horizontally onto PVC (polyvinyl chloride) substrates, gold (silicon chip coated with gold) or silicon supports. Monolayers transfer was carried out at a constant surface pressure of 5 or 18 mNm^{-1}. The transfer ratio for the LS films was no less than 0.95 for all substrates.

2.6 UV–vis reflection absorption spectroscopy

UV–vis reflection absorption spectra of Langmuir monolayers at the air–water interface were recorded in the 200–750 nm wavelength range using an AvaSpec–2048 FT–SPU (Avantes) fiber-optic spectrophotometer equipped with a 75 W DH-2000 deuterium-halogen light source and a CCD array detector. The UV–vis reflectometric probe with a fiber-optic diameter of 400 μm, combined with a 6–fiber irradiating bundle, was placed perpendicular to the studied surface at a distance of 2–3 mm. The signal reflected from the surface of the subphase prior to the deposition of the monolayer was used as a baseline.

2.7 Ultra high resolution scanning electron microscopy (SEM)

SEM imaging was performed using the Field Emission Scanning Electron Microscope Zeiss Supra 55 (FE-SEM, Carl Zeiss, Germany). Accelerating voltage was set at 2-15 kV with 4-6 mm working distance. Imaging was conducted using in-Lens secondary electron detector. For SEM studies, the LS films were transferred onto the cut silicon wafers.

2.8 X-Ray Studies

X-Ray patterns were acquired using Empyrean (Panalytical) diffractometer equipped with 1-D position-sensitive X'Celerator detector. Ni-filtered Cu Kα-radiation was employed. Calibration of angular scale in low-angle region was verified using fresh silver behenate

powder (Sigma Aldrich) [96]. Standard Bragg-Brentano (reflection) geometry was employed, allowing acquisition of out-of-plane diffraction, i.e. only planes parallel to the substrate are contributing. For X-ray studies, the LS films were transferred onto the PVC substrates.

Elemental analysis of LS film was performed by method of X-ray fluorescence spectroscopy using an X-ray Analytical Microscope (XGT 7200, Horiba, Japan), with a Rhodium (Rh) X-ray tube, a beam size 1.2 mm, tube voltage of 30 kV, and current of 0.15 mA under vacuum.

2.9 Electrochemical impedance spectroscopy

Electrochemical impedance spectroscopy measurements were performed with an IPC-compact homemade electronic potentiostat controlled by the Intelligent Potentiostat Control software (IPC-Compact ver. 8.65 developed at IPCE RAS, Moscow, Russia). The three-electrode cell was equipped with the working electrode (silicon chip coated with gold), an Ag/AgCl reference electrode, and a platinum mesh as an auxiliary electrode. A solution of $K_3[Fe(CN)_6]$ and $K_4[Fe(CN)_6]$ (1 mM each) prepared in 0.5 M KCl was used as an external redox-active probe. The cell was washed with deionized water and ethanol.

3. Results and discussion

3.1. Synthesis of DMSP, DMOP and DMNP

A synthetic approach to zinc complexes of (*trans*-A_2)BC-type porphyrinylphosphonate diesters was reported by us previously [93]. As shown in Scheme 1, **ZnDMSP, ZnDMOP** and **ZnDMNP** were prepared from 5,15-dimesitylporphyrin (**1a**) which was transformed in phosphonate diester **2a** in an overall yield of 45% by bromination with NBS followed by

the Pd-catalyzed phosphonylation reaction. The porphyrin **2a** was reacted with NBS to prepare bromide **3a**, which was involved in nucleophilic substitution reactions. This synthetic route was previously used by us for the preparation of functionalized 5,15-diphenylporphyrins and in preliminary experiments we try to synthesize the target compounds under the same experimental conditions. However, the reactivity of bromoporphyrins with respect to nucleophiles is found to be highly dependent on the nature of aryl substituents at the macrocyclic periphery and careful optimization of the reactions was needed to obtain the products in good yields.

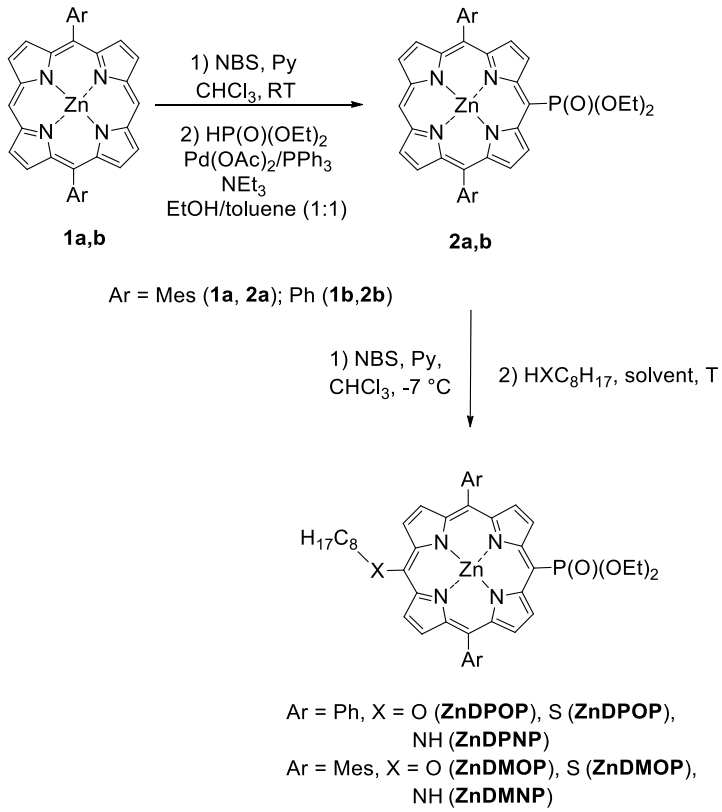

Scheme 1 Synthetic route to porphyrinylphosphonate diesters **ZnDMSP, ZnDMOP** and **ZnDMNP**.

Despite the fact that reactions of bromoporphyrins with alcohols commonly need palladium catalysts, the electron-deficient bromoporphyrins **3a** and **3b** reacted with alcohols and thioalcohols under catalyst-free conditions in the presence of cesium carbonate in DMA or without any solvent [93]. However, the reactions are non-selective and the target products are unstable under these reaction conditions. Thus, the product yield is highly dependent on the reaction time and temperature.

When the reaction of mesityl-substituted porphyrin **3a** with 1-octanol was run under the best conditions reported for the preparation of **ZnDPOP** (DMA, 90 °C, 2 h), the conversion of starting bromide **3a** was as low as 20% (Table 1, entry 1). The bromide **3a** was completely consumed only after 16 h at 120 °C (entry 2). However, three compounds were obtained and the reduced porphyrin **4** was a major product. The separation of these compounds by column chromatography on silica gel was impossible.

Table 1

S_NAr reaction of bromoporphyrin **3a** with *n*-octanol[a]

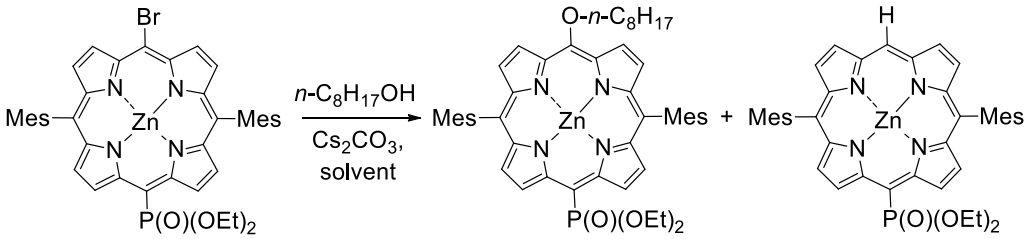

3a **ZnDMOP** **4**

Entry	Solvent	*T* [°C]	*t* [h]	Conversion [%][b]	Yield of **ZnDMOP** [%][b]

1	DMA	90	2	20	15
2	DMA	120	16	100	20
3[c]	DMA	120	12	14	7
4	*n*-octanol	95	2	100	(25)
5	*n*-octanol	70	16	25	25
6	*n*-octanol	85	4	100	(53)

[a] Reaction conditions: bromide **3a**, *n*-octanol (100 equiv.), cesium carbonate (3 equiv.) and solvent were heated under N_2 when monitored by MALDI-TOF MS. [b] Determined by ^{1}H NMR analysis. Isolated yields are given in parentheses. [c] Na_2CO_3 was employed as a base.

When sodium carbonate was employed as a base, the substitution was slow and accompanied by the hydrodebromination reaction (entry 3). The selective reaction was observed only in octanol, but the product yield was highly dependent on the reaction temperature because the **ZnDMOP** was unstable under these experimental conditions. For instance, the product was isolated in low yield after 2 h of the reaction at 95 °C despite complete conversion of the starting bromide **3a** (entry 4). When the temperature was decreased to 70 °C, the reaction was very slow (entry 5). The best result was obtained by reacting these compounds at 85 °C for 4 h when the product was isolated in 53% yield after chromatographic purification (entry 6).

The reaction of bromide **3a** with more nucleophilic octanethiol running without solvent was rapid but less selective as compared to the substitution of the bromine atom by octanol

(Scheme 2). Among many competing processes, the extensive hydrodebromination of starting bromide **3a** was observed as it was previously reported for the reaction of bromide **3b** with octanethiol [93]. When proceeded at room temperature, this reaction was completed in 2 h leading to an inseparable mixture of **ZnDMSP** and **4** in 2:1 molar ratio. The decrease of temperature up to 0 °C gave 55% yield of reduced porphyrin **4**. In contrast, by conducting the reaction at 120 °C, the hydrodebromination was suppressed and **ZnDMSP** was isolated in 68% yield when the reaction was stopped after 10 min.

The reaction of bromide **3a** with less nucleophilic *n*-octylamine was run under catalytic conditions developed previously for amination of **3b** (Scheme 3) [93]. The reaction smoothly proceeded in the presence $Pd(OAc)_2$/BINAP and cesium carbonate in refluxed toluene affording **ZnDMNP** in 63% yield.

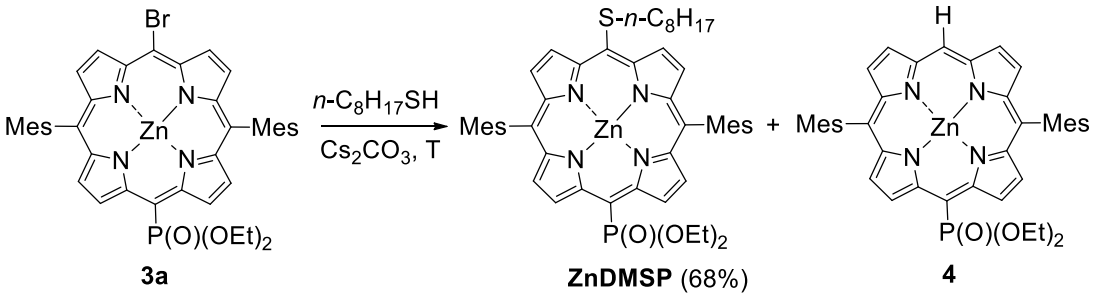

Scheme 2. Synthesis of **ZnDMSP**.

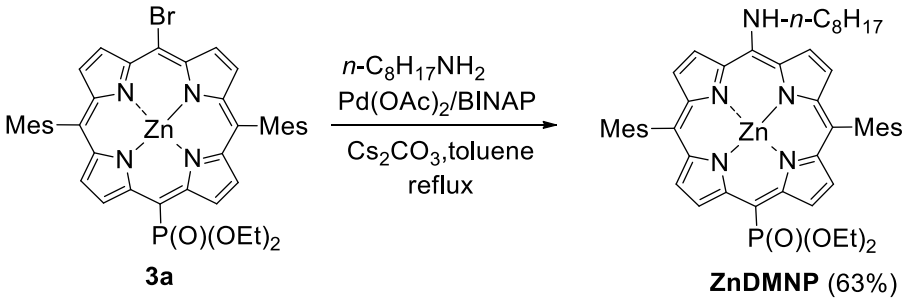

Scheme 3. Synthesis of porphyrin **ZnDMNP**.

Free base porphyrins **DMSP**, **DMOP** and **DMNP** were obtained in high yields by reacting their Zn complexes with concentrated hydrochloric acid in chloroform at room temperature.

All the studied compounds were unambiguously characterized by NMR, IR and UV–vis spectroscopies and MALDI-TOF analysis.

The electronic absorption spectra of obtained compounds are particularly interesting for our studies. They are shown in Fig. 2, S1 and S2 and spectroscopic data are summarized in Table S2. Two distinct regions of absorption is observed for all compounds as it is typical for porphyrins and have been interpreted by four-orbital model of Gouterman [97, 98]. Very strong Soret bands are centered at 420-430 nm and several less intensive Q bands appear in the 500-690 nm region. Low symmetry (D_{2h}) and the presence of polar substituents in the molecules impart some distinctive features to the spectra. The shape of absorbance curve of zinc complexes is more complicated as compared to those of conventional A_4-type metalloporphyrins with D_{4h} symmetry due to the loss of orbital degeneracy. Broadening of bands envelope or a split of the band was observed in the high-energy region of their UV–vis spectra. As shown in Fig. 2, the pseudo allowed Q transitions also showed complicated splitting pattern. Similar trends were also observed in the UV–vis spectra of free base porphyrins **DMSP**, **DMOP** and **DMNP**.

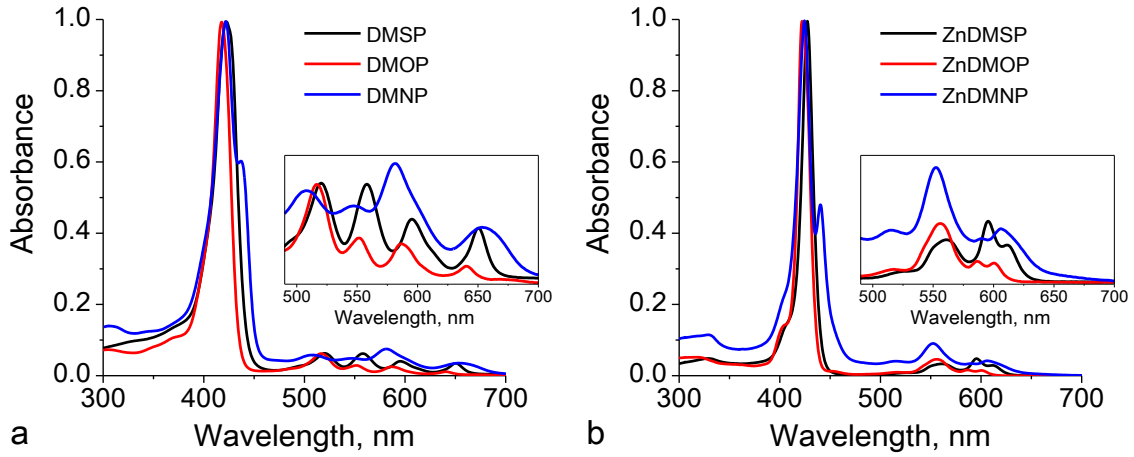

Fig. 2. Normalized UV–vis absorption spectra of **DMSP**, **DMOP** and **DMNP** in chloroform (a) and their Zn complexes in chloroform/methanol (2:1, v/v) solution (b) (c = 6.25 μM).

3.2. Metal ion binding by DMSP, DMOP and DMNP in solution

It is well known that in solution environment, including aqueous media, chelation of metal ions by four pyrrole nitrogen atoms of the porphyrin macrocycle leads to the change of their light absorbance and emission [17-21].

In chloroform, porphyrin **DMNP** bearing the most electron donating XC_8H_{17} substituent immediately responds to the addition of 2 equiv. of mercury(II), zinc(II), copper(II), lead(II) or cadmium(II) perchlorates by changing both absorption and emission of the studied solutions (Fig. 3, S3–S7). The metal complexation is manifested by a bathochromic shift of the Soret band and the appearance of three or four Q-bands of the complexes. The color of the solutions varies from light brown to green as shown in Fig. 3. Efficient fluorescence quenching is observed for all metal ions except Zn^{2+}. This quenching can be detected even visually upon irradiation of the solutions with a 365 nm diode.

As shown in Fig. 3a and S3–S7, the selectivity of **DMSP** and **DMOP** with respect to toxic metals in chloroform is a bit higher compared to that of **DMNP** but still far from any practical interest in sensing because these ligands chelate all studied metal ions except Cd^{2+}. In the presence of Cu^{2+}, hypsochromic shifts of the Soret band were recorded for both ligands, while Zn^{2+} ions caused bathochromic shifts, that is typical for the formation of in-plane and border-line porphyrin metal complexes, respectively [20].

Quenching of **DMSP** and **DMOP** fluorescence was observed after addition of Cu^{2+}, Pb^{2+} and Hg^{2+} cations (Fig. 3b and c, respectively). In contrast, addition of zinc(II) perchlorate results in emissive solutions (Fig. 3b, c). The heteroatom substituent influenced not only the shift of the absorption and emission maxima (Fig. 3) but also the time needed to reach the equilibrium conditions. For instance, the complexation of zinc(II) and copper(II) ions by **DMSP** and **DMOP** has taken a rather long time (60 min) (Fig. S3–S6) as it was previously observed for many water-soluble porphyrins [20].

It has to be noted, that all three ligands being coordinated to Hg^{2+} ions afford stable complexes, in which the bulky metal ion is located above the macrocycle plane as evidenced by a large bathochromic shift of the Soret band, typical for out-of-plane porphyrin complexes [20, 99, 100]. The fluorescence quenching after addition of mercury(II) perchlorate is also observed for all three studied compounds (Fig. 3b–d).

The protonation of **DMSP**, **DMOP**, and **DMNP** also leads to fluorescence quenching, but can be distinguished from the complexation reactions *via* more pronounced bathochromic shifts of the Soret band (Table 2, Fig. S8–S10).

Thus, despite specific structural features, our ligands are efficient dual-channel molecular probes of Hg^{2+} ions in chloroform. However, they exhibit a low selectivity with

respect to this analyte. The heteroatom substituent influences the coordination properties of porphyrinylphosphonate diesters. This can be caused by electronic effects of the substituents and/or a preliminary coordination of the cations to the heteroatoms located at the periphery of the macrocycle.

Table 2. Soret and Q-absorption bands (nm) for the porphyrins **DMSP**, **DMOP** and **DMNP** in chloroform solution upon addition of metal perchlorate

Porphyrin /Analyte	Soret band	Q bands			
DMSP	421	520	558	595	650
H^+	450	-	545	598	652
Hg^{2+}	445	-	550	590	646
Cu^{2+}	419 443	-	550	587	647
Zn^{2+}	428	520	560	595	648
Pb^{2+}	424 443	517	557	593	647
Cd^{2+}	422	520	558	595	650
DMOP	418	517	551	587	640
H^+	440	-	537	584	634
Hg^{2+}	433	-	537	579	628

Cu^{2+}	415	-	542	577	628
Zn^{2+}	422	553	585	600	629
Pb^{2+}	424	516	551	582	628
Cd^{2+}	418	517	551	587	640
DMNP	421 437	507	548	582	656
H^{+}	436	499	534	597	654
Hg^{2+}	430	-	500	606	657
Cu^{2+}	431	-	502	575	655
Zn^{2+}	424	502	553	605	657
Pb^{2+}	430	-	499	606	658
Cd^{2+}	421	507	551	583	657

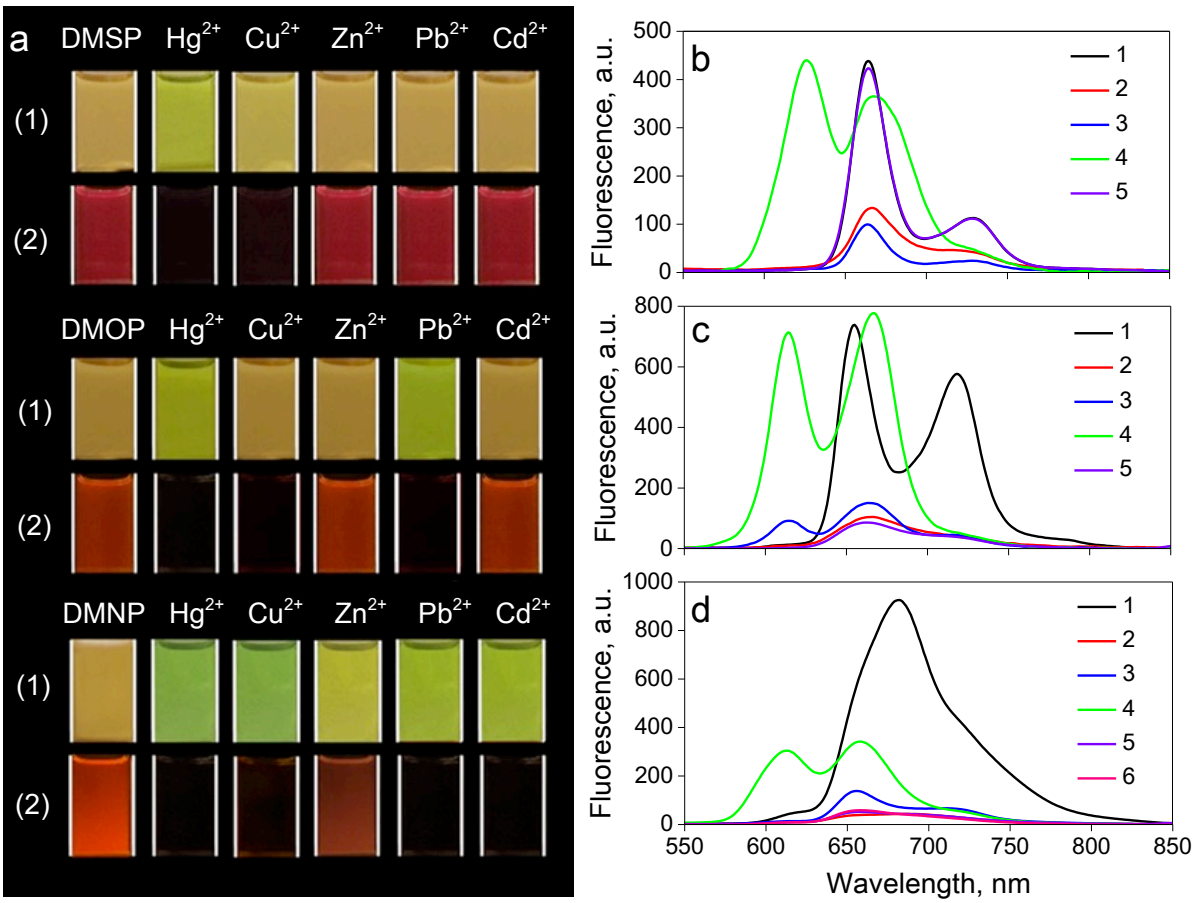

Fig. 3. (a) Cation-induced color changes of **DMSP**, **DMOP** and **DMNP** chloroform solutions upon addition of metal perchlorates before (*1*) and after (*2*) diode irradiation (365 nm), equilibration time was 60 min. Evolution of the fluorescence (b - d) spectra (λ_{ex} = 420 nm) of **DMSP** (b, *1*), **DMOP** (c, *1*) and **DMNP** (d, *1*) upon addition of metal perchlorates: for **DMSP** and **DMOP** (*2*) 3 equiv. of Hg^{2+}, (*3*) 1 equiv. of Cu^{2+}, (*4*) 1 equiv. of Zn^{2+}, (*5*) 3 equiv. of Pb^{2+} and for **DMNP** (*2*) 2 equiv. of Hg^{2+}, (*3*) 2 equiv. of Cu^{2+}, (*4*) 2 equiv. of Zn^{2+}, (*5*) 2 equiv. of Pb^{2+}, (*6*) 2 equiv. of Cd^{2+} in chloroform solutions, all spectra are corrected for dilution effects.

3.3. Monolayers of porphyrins DMOP, DMSP and DMNP on the water surface

Porphyrin monolayers on the surface of deionized water were formed according to

Langmuir technique. Surface pressure–area (π–A) isotherms of **DMOP**, **DMSP** and **DMNP** are depicted in Fig. 4a.

Compression isotherms of **DMOP** and **DMSP** monolayers are quite similar both in the shape and in the values of molecular areas. The molecular area at the «lift-off points» of the isotherms (i.e., at the points where the surface pressure π starts to rise) was calculated to be 150 $Å^2$/molecule, which is smaller than the expected value for the face-on orientation of the macrocycle (~ 225–250 $Å^2$/molecule) [64, 101]. Thus, when the monolayer is compressed, the molecules adopt an inclined orientation (Fig. 4b), which is greatly facilitated by the substituent pattern of the macrocycles, particularly by the presence of the polar hydrophilic diethoxyphosphoryl group and the opposite hydrophobic substituent with a hydrocarbon chain. This slipped stack-of-card orientation of the molecules is typical for monolayers of amphiphilic porphyrins at the air–water interfaces, but the values of "lift-off points" in these films commonly lie in the range of 70–120 $Å^2$/molecule [101]. An increase of this value up to 150 $Å^2$/molecule for **DMOP** and **DMSP** is likely due to steric effects of bulky mesityl and phosphorous-containing substituents.

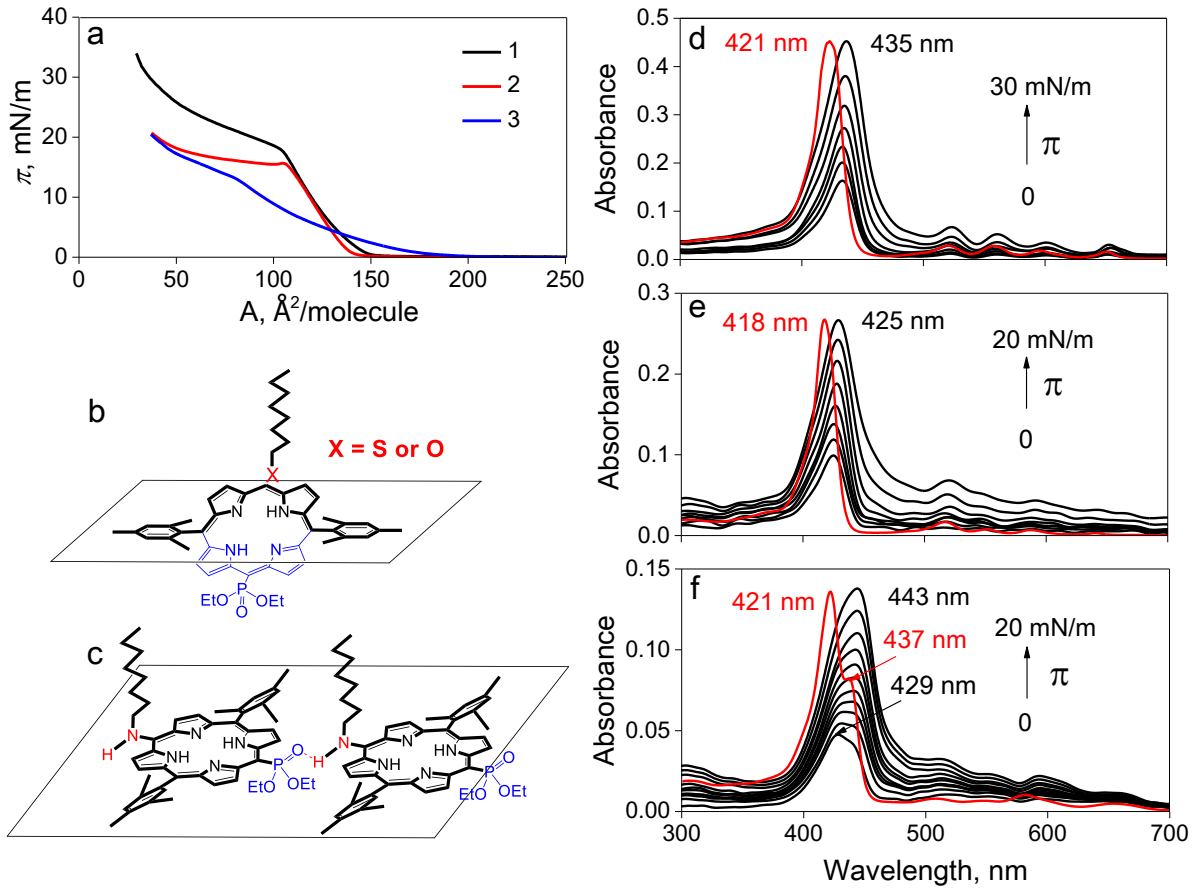

Fig. 4. (a) Surface pressure *vs* area isotherms for the monolayers of **DMSP** (*1*), **DMOP** (*2*) and **DMNP** (*3*) on the pure water surface. (b) Schematic illustration of the proposed molecular orientation of **DMSP** and **DMOP** in the monolayer on the pure water surface at 110–125 Å^2/molecule. (c) Schematic illustration of the proposed molecular orientation of **DMNP** in the monolayer on the pure water surface at 200 Å^2/molecule. (d-f) *In situ* absorption spectra for the monolayers of **DMSP** (d), **DMOP** (e) and **DMNP** (f) on the pure water surface under compression. Spectra of the porphyrins in chloroform solution are also shown for comparison (red).

The rapid increase of the surface pressure upon monolayer compression likely indicates a decrease in the molecular inclination angle relative to the surface normal. After reaching

the dense packing, which observed at the pressure of 18–20 mN m^{-1} and the surface area of 110 $Å^2$/molecule, the monolayers are reorganized, as evidenced by clearly defined "kink-points". The monolayer compressibility significantly increases probably due to squeezing out of the porphyrin molecules leading to the formation of floating films composed of a few monolayers or nano-sized discrete 3D aggregates [85, 102].

To gain a deeper insight into the structural organization of the monolayers, their reflection absorption spectra were recorded and compared to those of the porphyrins in solution environment. The aggregation of porphyrin molecules in a monolayer is evidenced by broadening and shifting of the Soret band, as predicted by exciton theory [103]. The absorption spectra of **DMOP** and **DMSP** and their monolayers are presented in Fig. 4d and 4e, respectively. The Soret bands of the monolayers are only slightly broadened and red-shifted (7 and 14 nm, respectively) relative to those of porphyrins in chloroform solution [104]. It worth to note, that the Soret bands of both floating films are much narrower compared to that of **TPP** monolayers [66]. Moreover, when **DMOP** and **DMSP** monolayers are compressed, the emergence of new bands in the high-energy region was not observed in contrast to the monolayers of many other porphyrins with D_{2h} symmetry in which excitonic interactions between the porphyrin excited states were observed [69, 104-107].

Considering these spectral data, the self-assembly of **DMOP** and **DMSP** into weak J-aggregates [108] through π–π interactions cannot be definitively excluded because small bathochromic shifts of the absorption maxima of the Soret bands are observed. However, these shifts may also be induced by a change in the environmental polarity [64]. In any case, we can safely conclude that bulky substituents of the porphyrin macrocycle prevent the formation of strong porphyrin aggregates in the studied monolayers.

In the case of the **DMNP** monolayer, the shape of the compression isotherm drastically differs from the π–A curves for **DMOP** and **DMSP** floating films (Fig. 4a). The value of surface area (200 $Å^2$/molecule) at the «lift-off point» is closer to limiting areas of monolayers with the face-on orientation of tetrapyrrolic macrocycles. A plausible rationale for this finding is a change in the orientation of porphyrin molecules in the monolayer due to intermolecular hydrogen bonding of octylamino and diethoxyphosphoryl groups leading to the formation of porphyrin chains (Fig. 4c). In these supramolecular aggregates, the tetrapyrrolic macrocycles are almost parallel to the liquid surface at low level of surface coverage. This hydrogen bonding strongly influences the structure of the monolayer during its compression. In contrast to **DMOP** and **DMSP** monolayers, a slow slope variation is observed before and after a slightly marked kink at 80 $Å^2$. The behavior of **DMNP** holds certain implications to previous studies of porphyrin monolayers, in which the influence of hydrogen bonding on the structure of Langmuir monolayers was observed [68]. UV–vis spectrum of this monolayer is quite similar to that recorded for this porphyrin in chloroform solution but broadened and red-shifted (6–8 nm). Interestingly, for this floating film, the shape and position of Soret and Q bands are dependent on the compression pressure, presumably due to the change in the orientation and packing of the macrocycles with the increase of surface pressure.

Thus, being deposited on the water surface by Langmuir technique, **DMOP**, **DMSP** and **DMNP** form stable monolayers in which the porphyrin molecules are ordered and initial surface areas are as high as 150–200 $Å^2$/molecule. The heteroatom-containing substituent influences the structural organization of the monolayers.

3.4. Sensing properties of DMOP, DMSP and DMNP monolayers

The complexation of interfering mercury(II), copper(II), zinc(II) and lead(II) ions by **DMSP** monolayer was studied by comparing UV–vis spectra and compressing isotherms of the monolayer formed on the surface of water and aqueous solutions of the metal perchlorates (Fig. 5a, b). For each studied analyte, several UV–vis spectra were recorded at the surface pressure of 15 mN m^{-1} to ensure a complete complexation of the metals (15–60 min). The Cu^{2+}, Zn^{2+} and Pb^{2+} ions appear to be coordinated to only the peripheral donor heteroatoms, which is confirmed by 1) the only small spectral difference between corresponding UV–vis spectra and 2) a shift of the isotherms towards large areas in the presence of metal ions owing to electrostatic repulsion of cations in the floating films. This coordination modes of functionalized porphyrins was already observed in **DPOP** monolayers formed on the surface of aqueous solution of zinc(II) perchlorate [93]. In contrast, Hg^{2+} ions seem to be ligated by four pyrrolic nitrogen atoms of the porphyrin macrocycle, which follows from a significant bathochromic shift of the Soret band and the changes in the spectrum shape in the Q region. The formation of the mercury(II) complex with porphyrin leads to the liberation of two protons and affords a neutral species with porphyrin to Hg^{2+} ratio of 1:1 [100, 109, 110]. The isotherm of the ligand shifts towards smaller molecular areas and the monolayer rigidity is greatly increased probably due to a high tendency of porphyrins to form with mercury(II) ions sandwich-type complexes (Fig. S11) [100].

In the case of **DMOP,** the introduction of copper (II) and zinc(II) cations does not shift the compression isotherms and the absorption spectrum remains almost unchanged (Fig. 5b, c). It seems that both metals do not form any complexes with the porphyrin ligand organized in the monolayer, at least after 60 min of the contact. These data lead us to a

tentative conclusion that the oxygen atom of the octanoxy substituent does not participate in the complexation of these metals probably owing to the conjugation of the oxygen lone pair with the aromatic macrocycle.

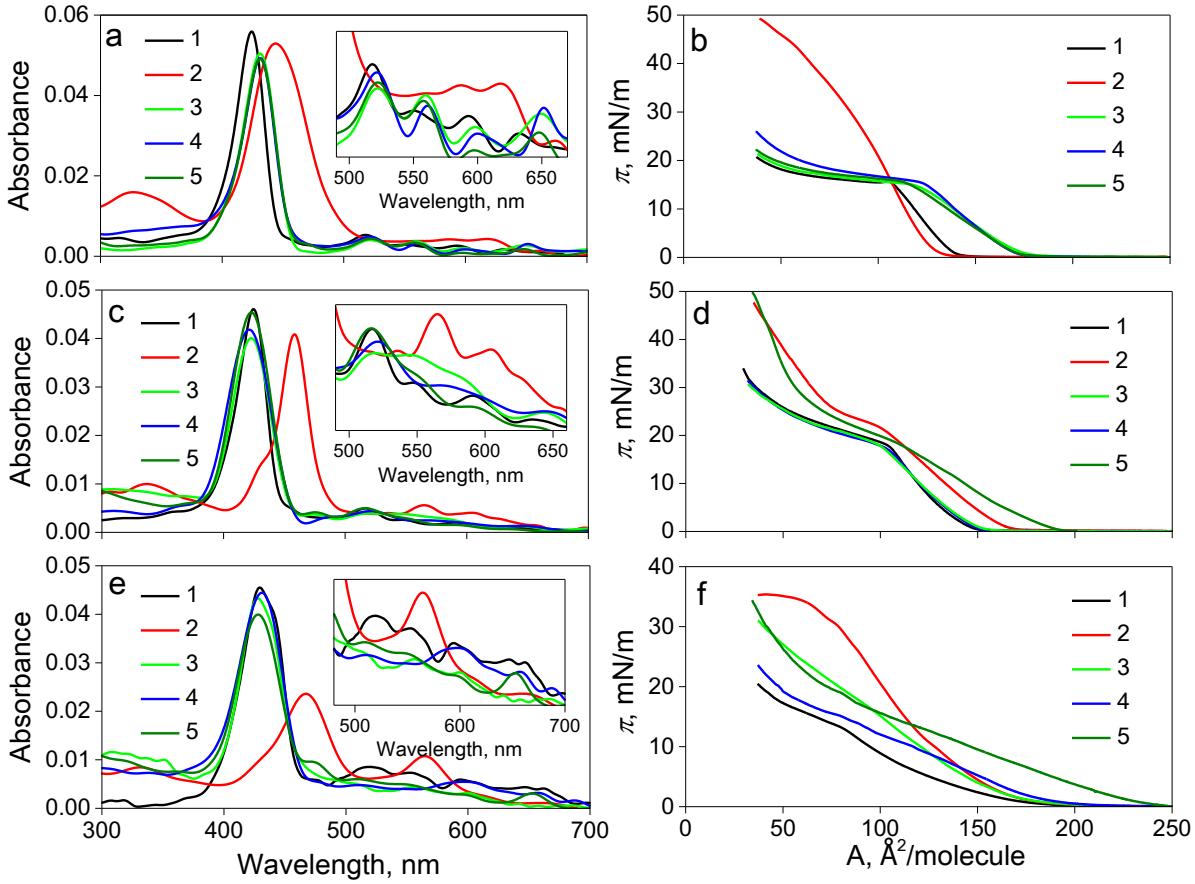

Fig. 5. *In situ* absorption spectra (a, c, e) and surface pressure vs area isotherms (b, d, f) for the monolayers of **DMSP** (a, b), **DMOP** (c, d) and **DMNP** (e, f) on the surface of pure water (1) and 1 mM aqueous solutions of $Hg(ClO_4)_2$ (2), $Cu(ClO_4)_2$ (3), $Zn(ClO_4)_2$ (4) and $Pb(ClO_4)_2$ (5). Equilibration time before compression was 15 min (1) and 60 min (2–5), respectively. *In situ* absorption spectra are recorded at surface pressure 15 mN m^{-1}.

In contrast, in the presence of lead(II) cations, the compression isotherm of the **DMOP** monolayer is shifted toward large areas. This shift is accompanied by an increase in the

monolayer rigidity. The intact position of the maximum of the Soret band indicates that only donor centers at the macrocycle periphery are coordinated to the metal ion as it was observed for **DMSP** monolayer (Fig. 5a, b).

Introduction of mercury(II) cations into the aqueous subphase leads to the complexation of this metal by the macrocycle as unambiguously indicated by a bathochromic shift of the Soret band and the spectral changes in the Q region of the spectrum. It is worth to note that the compression isotherm of this complex is very similar to that of Pb^{2+} complex with **DMOP** and is displaced to large molecular areas in comparison with Hg^{2+} complex with **DMSP**.

Sensing properties of **DMNP** and **DMSP** were alike in all their basic features with the exception that compression isotherms of **DMNP** on the surface of subphase containing Cu^{2+}, Zn^{2+} and Pb^{2+} ions exhibited larger molecular areas at the «lift-off points» and slower slope variations. It seems that both the nitrogen atom of the octylamine group and the phosphoryl oxygen atom are coordinated to the metal ions in the monolayer inducing a mainly horizontal orientation of the macrocycles at a low density of the monolayers (Fig. 5f).

It has to be noted that analogous switching in the coordination mode of porphyrin ligand was observed for **TPyP** in a solution environment [89]. In ethanol, four pyrrolic nitrogen atoms of **TPyP** are chelated to Hg^{2+} ions, but not to Cu^{2+} cations. In the later complex, only pyridine nitrogen atoms participate in the binding of Cu^{2+} ions. The same coordination modes of these metal ions were proposed by the authors for LS films formed by **TPyP** but experimental evidences of Hg^{2+} coordination by the macrocycle in the film were quite delicate.

In conclusion, being organized in Langmuir monolayers, porphyrins **DMOP, DMSP** and **DMNP** develop selective spectrophotometric responses on the presence of mercury(II) ions in the aqueous subphase. In these sensory systems, only Hg^{2+} ions are coordinated to the tetrapyrrolic macrocycle while other metals (Cu^{2+}, Zn^{2+} and Pb^{2+}) are ligated to the peripheral donor sites if at all.

3.5. Langmuir-Schaefer films of DMOP, DMSP and DMNP

The monolayers of porphyrinylphosphonate **DMOP**, **DMSP** and **DMNP** were transferred onto a PVC support using the LS method. The deposition was performed at two different surface pressures (5 and 18 mN m^{-1}) and optic properties of the films were monitored by absorption and fluorescence spectroscopies (Fig. 6, S13–S14).

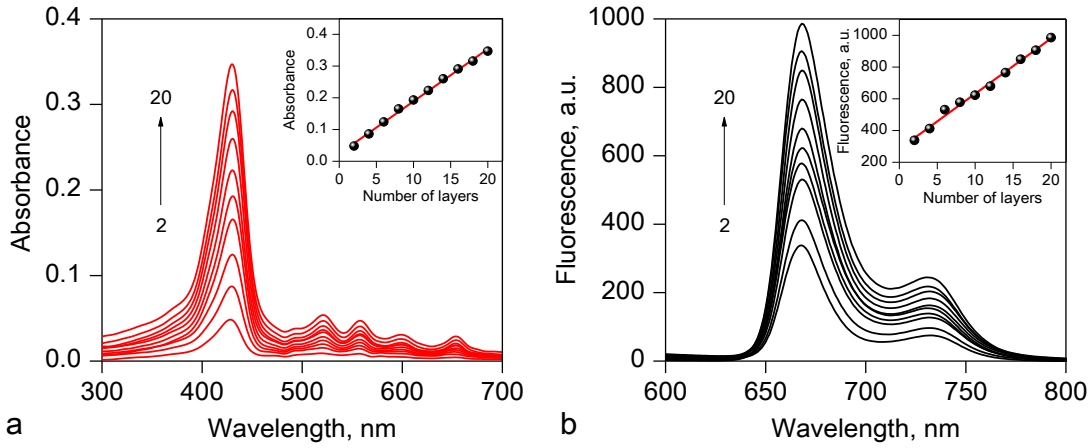

Fig. 6. UV–vis absorption (a) and fluorescence (b) spectra for LS film of **DMSP** deposited onto a PVC substrate from the pure water surface at 5 mN m^{-1} (λ_{ex} = 420 nm). Inset shows the dependence of the absorbance (a) and fluorescence (b) intensity *vs* the number of layers in the LS film at λ = 425 (a) and 668 (b) nm.

In the absorption spectra, the linear increase of the B-band and Q-band intensities with the

number of transferred layers was observed for all three films under both transfer conditions. This evidences a high degree of the monolayer transfer. More importantly, the intensities of the emission bands were high and increased regularly for **DMOP** and **DMSP** films, confirming the absence of strong aggregation in these multilayer films in contrast to many LS films of amphiphilic porphyrins reported previously [70]. The emission of the **DMNP** film was less intensive and its increase with the enhancement of film thickness was less regular probably due to the aggregation of porphyrin molecules as it was observed for its Langmuir monolayer (Fig. 4f).

The structure of 30-layer LS films of **DMSP**, **DMOP** and **DMNP** transferred onto PVC substrate at 5 and 18 mN m^{-1} was investigated by XRD analysis. Only **DMSP** film deposited at 18 mN m^{-1} displayed Bragg peaks (Fig. S15) and their interpretation was not straightforward. Two reflections with similar intensities appear at 3.42° and 6.89°, corresponding to distances of 25.75 Å and 12.81 Å, respectively. Such a pattern indicates a high level of local molecular organization in the film showing that this material displays at least layer structure. As for the films of **DMOP** and **DMNP** porphyrins, which do not give any Bragg reflections, it can be assumed that after the transfer of monolayers onto solid supports, a structural rearrangement occurs leading to the formation of amorphous domains or very small microcrystallites.

Morphology of LS films was investigated by scanning electron microscopy (SEM) (Fig. 7). The films structurally differ one from other. Both **DMSP** and **DMOP** films transferred at 5 mN m^{-1} form networks which uniformly cover the surface of the substrate over large areas (Fig. 7a, b). Nevertheless, density of **DMOP** film is higher than that of its sulfur-containing analogue. SEM image of **DMNP** film shows that this material has a complex morphological pattern. Two types of structures are apparently formed in the film: 1) homogeneous with inclined orientation of macrocycles and 2) chain-type with a planar orientation of macrocycles, which is formed *via*

hydrogen bonds between >NH and $–P(O)(OEt)_2$ groups. (Fig. 7c). As the transfer pressure increases to 18 mN m^{-1}, the structural elements of films become more consolidated (Fig. 7d, e, f).

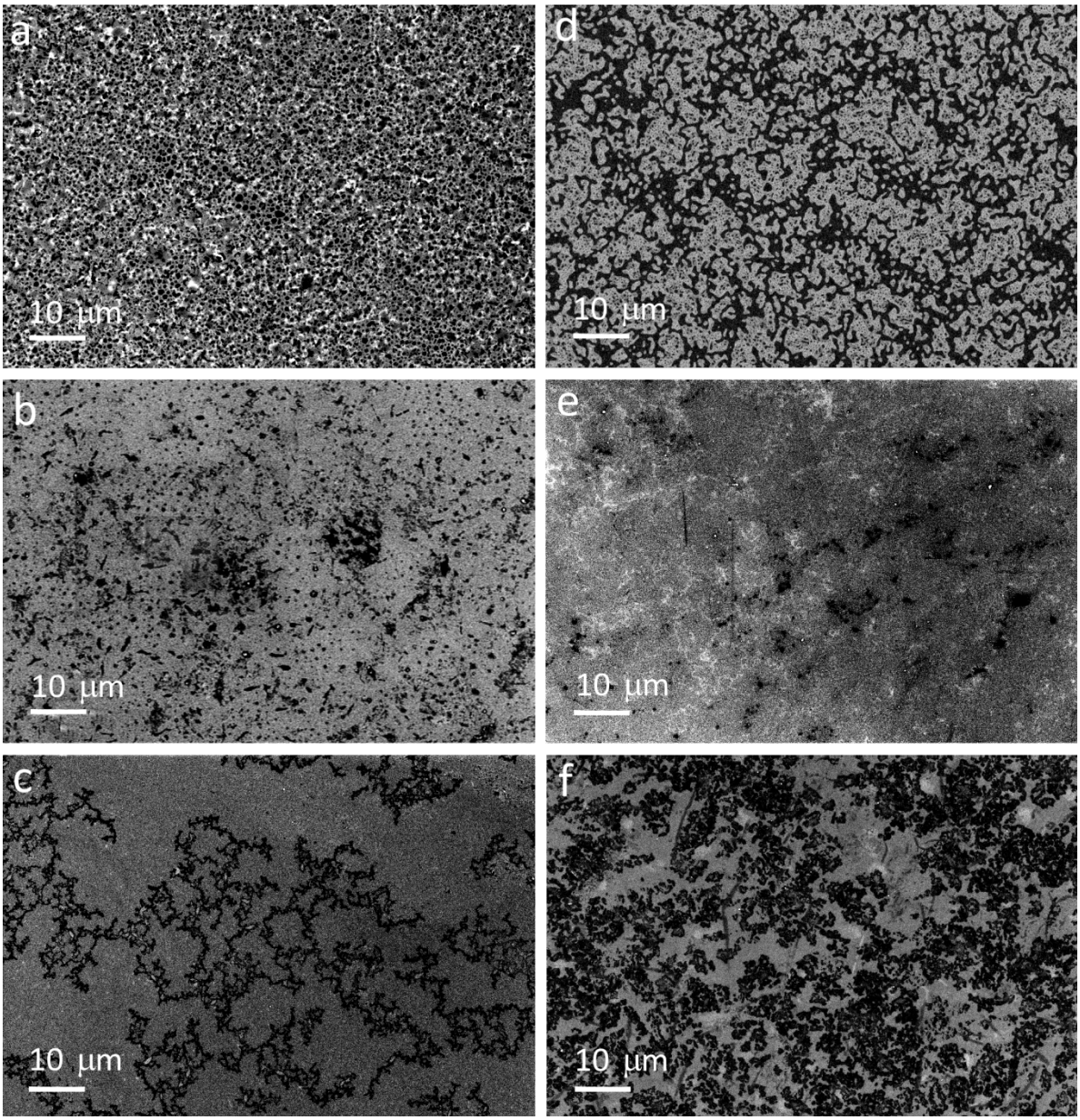

Fig. 7. SEM images of 5-layer LS films of **DMSP** (a, d), **DMOP** (b, e) and **DMNP** (c, f) deposited onto a cut silicon wafer at a surface pressure of 5 (a, b, c) and 18 (d, e, f) mN m^{-1} from the deionized water surface.

The LB and LS techniques are traditionally appreciated in material chemistry as convenient methods for fabrication of highly uniform and dense films with a high predetermine composition, architecture and thickness [58, 59, 61]. However, for some technical applications such as sensing, for instance, these features are actually detrimental to performance causing a slow diffusion of an analyte to reaction centers. Therefore, morphology modifications of the LB and LS films, which afford an increase of their surface area, are advantageous for these applications. For instance, the ultra-rapid transfer of LB monolayers was developed to form non-uniformed films consisting of nano-structured domains. This sensing material exhibited a higher sensitivity as compared to conventional LB films due to the enhanced surface area of the porous film assembly [111]. The porphyrinylphosphonate diesters can be organized in perforated film assemblies by simple LS technique due to their appropriate molecular design. The observed features of the surface morphology of **DMOP**, **DMSP** and **DMNP** films can be a consequence of substrate-induced transformations or slow dewetting of transferred monolayers containing water molecules due to their hydrogen bonding to polar substituents at the macrocycle periphery [25].

DMOP, **DMSP** and **DMNP** monolayers formed at 5 mN m^{-1} were also transferred onto the gold surface and investigated by electrochemical impedance spectroscopy, which allows for estimation of the film permeability by measuring the charge transfer resistance between the gold electrode and an external redox couple containing electrolyte (Fig. 8, Table 3).

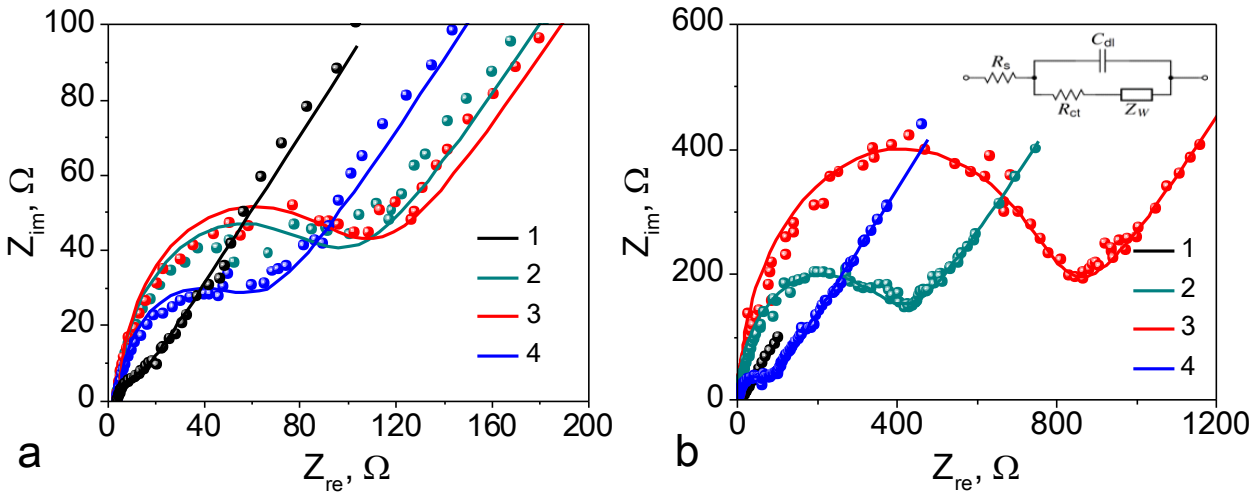

Fig. 8. Nyquist plots (hodographs) of a pure gold electrode (*1*); gold electrode coated with a single layer LS films of **DMSP** (*2*), **DMOP** (*3*) and **DMNP** (*4*) transferred at a surface pressure of 5 mN m^{-1} from the surface of deionized water before (a) and after (b) exposure in 0.1 mM $Hg(ClO_4)_2$ aqueous solution for 10 min. The inset shows the equivalent Randles circuit used for EIS data modeling.

Table 3. Electrochemical parameters obtained for one-layer LS films of **DMSP**, **DMOP** and **DMNP** on a gold electrode from mathematical modeling of the corresponding Nyquist plots, according to the equivalent Randles circuit presented on the inset of Fig. 8b.

System	R_s[a] (Ω)	C_{dl}[b] (μF cm^2)	R_{ct}[c] (Ω cm^2)	Z_W (Ω $s^{1/2}$)
Au	4.0	12.6	7.6	236.7
Au/ **DMSP**	5.0	17.5	81.3	248.7
Au/ **DMOP**	5.2	15.7	90.8	255.0

Au/ **DMNP**	5.0	14.0	49.0	274.3
Au/ **DMSP**/Hg^{2+}	5.2	14.2	358.1	455.0
Au/ **DMOP**/Hg^{2+}	4.5	14.5	764.4	319.0
Au/ **DMNP**/Hg^{2+}	5.1	12.5	52.3	277.4

[a]R_s: electrolyte resistance. [b]C_{dl}: electrical double layer capacity. [c]R_{ct}: charge transfer resistance at the electrode/electrolyte interface. [d]Z_W: Warburg diffusion element.

Comparing LS films of **DMSP** and **DMOP** (Fig. 8a, Table 3), the latter shows higher charge transfer resistance. This is consistent with SEM data obtained for the thicker films on PVC support formed at the same deposition surface pressure (Fig. 7).

The fact that charge transfer resistance is low for the **DMNP** film indicates the presence of significant number of defects in this film. This finding also correlates with the SEM image of the multilayer **DMNP** film on PVC, which demonstrate its high inhomogeneity (Fig. 7).

When the **DMSP** and **DMOP** films were immersed in aqueous solution of mercury(II) perchlorate for 10 min, the metal-bound ligands gave rise to better organized insulating layers as indicated a significant increase of the charge-transfer resistance (Fig. 8b, Table 3). Interestingly, when **DMNP** film was exposed to Hg^{2+} ions, the charge transfer resistance does not change, likely due to a structural difference of the monolayers formed by **DMNP** and other studied porphyrins.

Thus, porphyrinylphosphonates **DMOP, DMSP** and **DMNP** form stable, colored and emissive LS films on the surface of PVC. The perforated structure of these films is advantageous

for their sensing applications. Their emissive properties and their morphology are dependent on the nature of heteroatom substituent at the macrocyclic periphery. The LS films formed by porphyrins **DMOP** and **DMSP** seem to be more appropriate for developing of solid film sensors owing to their higher emission.

3.6. Sensing properties of DMOP, DMSP and DMNP films

The LS films formed by three studied porphyrins on the surface of PVC support offer selective spectrophotometric responses on the presence of mercury(II) ions as Langmuir monolayers formed by these compounds at the air–water interface. Exposure of 10-layer **DMOP**, **DMSP** and **DMNP** films to 0.1 mM solution of mercury(II) perchlorate for 30 min led to a bathochromic shift of the Soret band (Fig. 9a, c, e). Moreover, using these LS films, the presence of the Hg^{2+} ions can be detected by emission spectroscopy owing to almost complete fluorescence quenching upon the complex formation (Fig. 9 b, d, f).

The sensors can be regenerated by the treatment with an acidified aqueous solution (pH = 2) as shown in Fig. 9.

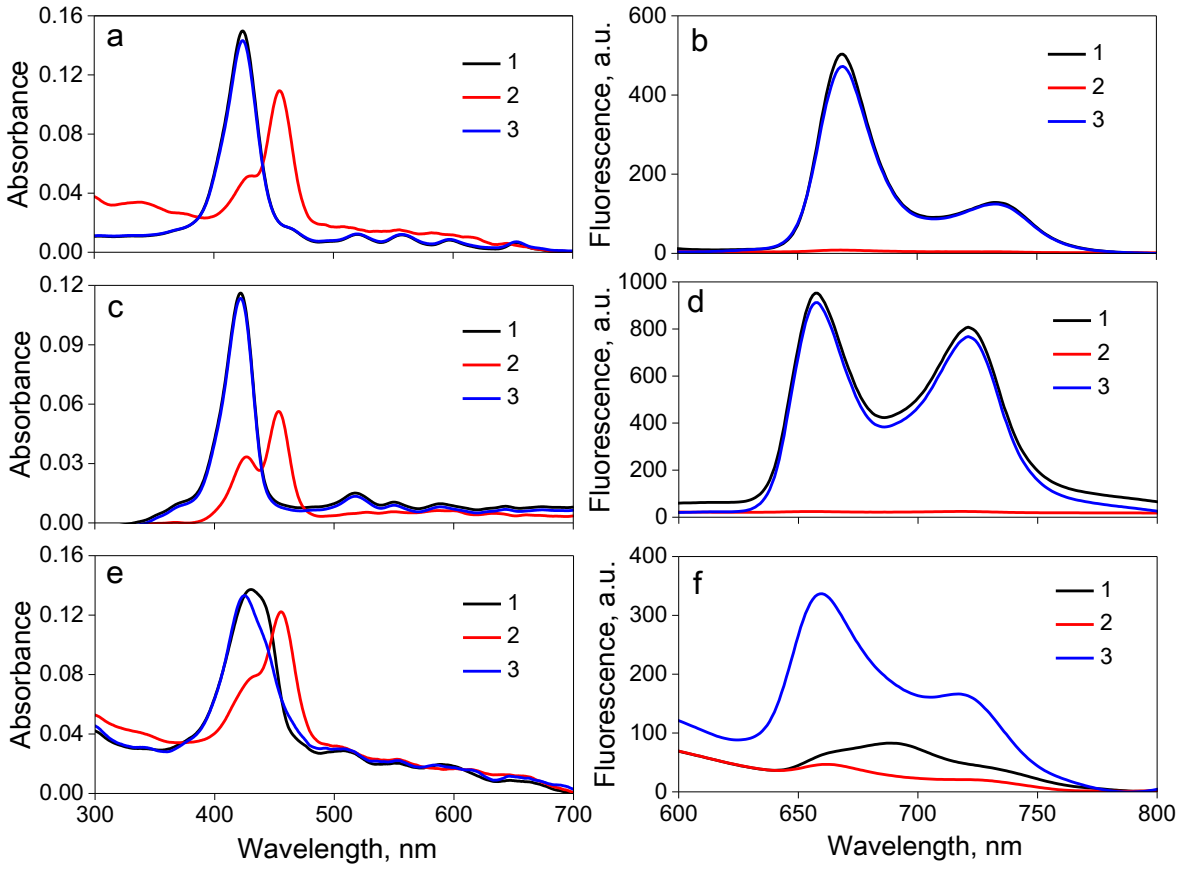

Fig. 9. UV–vis absorption (a, c, e) and fluorescence (b, d, f) spectra (λ_{ex} = 420 nm) of 10-layer LS films of **DMSP** (a, b), **DMOP** (c, d) and **DMNP** (e, f) deposited onto a PVC substrates from pure water surface at 5 mN m^{-1} (*1*) and immersed in 0.1 mM aqueous solution of $Hg(ClO_4)_2$ for 30 min (*2*) followed by washing by acidified aqueous solution (pH 2) for 3 min (*3*).

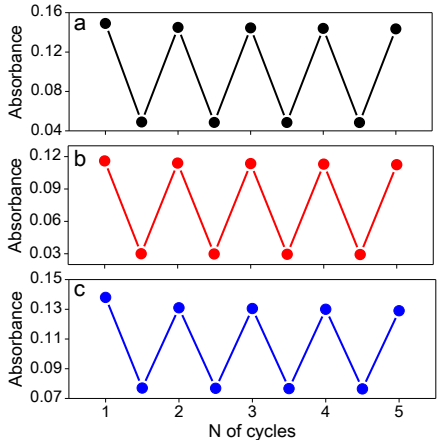

Fig. 10. Changes of absorbance intensity at 424 nm (**DMSP**, a), 421 nm (**DMOP**, b) and 424 nm (**DMNP**, c) during five consecutive analyses of Hg^{2+} ions in aqueous samples (10-layer LS film; exposition to 0.1 mM aqueous solution of $Hg(ClO_4)_2$ for 30 min; washing by an acidic solution with pH 2 for 2 min).

Interestingly, the absorbance and emission spectra of regenerated films were similar to those of pristine materials only in the case of **DMOP** and **DMSP** sensors. For the film of amino-substituted porphyrin **DMNP**, the Soret band was more structured. Moreover, a significant increase of emission intensity was observed after the sensor regeneration (Fig. 9f). These spectral changes were ascribed to the structural reorganization of the **DMNP** film under acidic conditions. Intermolecular hydrogen bonding plays a crucial role in the self-assembly of **DMNP** molecules in the Langmuir monolayers and likely in LS films because the morphology of **DMNP** film significantly differs from those of **DMOP** and **DMSP** films (Fig. 7). The treatment of **DMNP** sensor by an acidic solution leads to a removal of Hg^{2+} ions and the protonation of the octylamino group. The later process can induce significant structural changes of porphyrin monolayers due to strong electrostatic repulsions of positively charged porphyrin molecules as it was observed for **DMOP, DMSP** and **DMNP** monolayers after the complexation of Zn^{2+}, Cu^{2+} and Pb^{2+} ions by the

ligands (Fig. 5).

Interestingly, the regenerated **DMNP** film preserves its sensory properties as do the recovered **DMOP** and **DMSP** sensors. The **DMOP**, **DMSP** and **DMNP** films can be regenerated at least 5 times without loss of their efficiency (Fig. 10).

Next, it was demonstrated that convenient naked-eye analysis of Hg^{2+} ions is possible by **DMOP, DMSP** and **DMNP** films composed of 30 porphyrin layers transferred at 5 mN m^{-1} (Fig. 11a). These films can be also regenerated by treatment with diluted hydrochloric acid (pH = 2). The presence of mercury(II) ions in **DMSP** film after the analysis and their total removal after washing of the sensor were confirmed by X-ray fluorescence analysis (Fig. 11b, c).

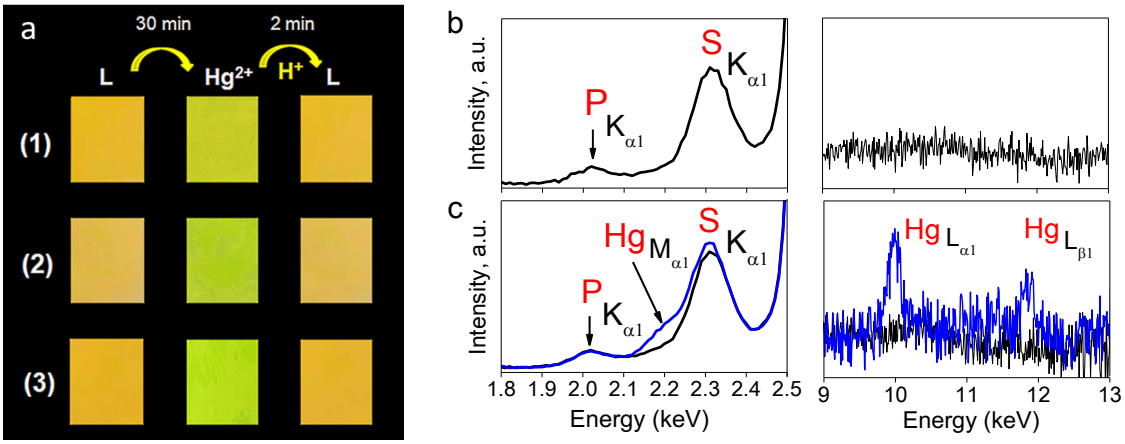

Fig. 11. (a) Cation-induced color changes of 30-layer LS film of: **DMSP** (*1*), **DMOP** (*2*) and **DMNP** (*3*), transferred onto a PVC substrate at a surface pressure of 5 mN m^{-1} from the pure water surface. X-ray fluorescence spectra of 30-layer LS film of **DMSP** transferred onto a PVC substrate at a surface pressure of 5 mN m^{-1} from the pure water surface (a), LS film after exposure to 1 mM $Hg(ClO_4)_2$ aqueous solution (b – blue line); LS films **DMSP/Hg^{2+}** that have been regenerated using acidified aqueous solution (b – black lines).

The effect of Hg^{2+} ions on structure of **DMSP** 30-layer LS films transferred onto solid substrate at 18 mN m^{-1}, was also investigated by XRD analysis. As mention above, only this pattern film shows Bragg reflections (Fig. S15). Like the pristine material, the film treated with Hg^{2+} ions displays two peaks with equal intensity. They appear at 4.22° and 5.30°, which correspond to distances of 20.92 Å and 16.64 Å, respectively (Fig. S15). These data evidence a structural reorganization of the ordered sensing film after the complexation of the metal ions.

Instrumental LOD of all thin-film sensors was as low as 10^{-8} M (2 ppb) (Fig. S18–S19), which corresponds to the maximum contamination level (of 2 ppb) for Hg^{2+} ions in drinking water recommended by EPA [5]. Moreover, interfering Cu^{2+}, Zn^{2+}, Cd^{2+} and Pb^{2+} ions do not significantly disturb the analyses of Hg^{2+} cations. The best results in cross-selectivity experiments were obtained with **DMSP** film as shown in Fig. 12 and Fig. S20.

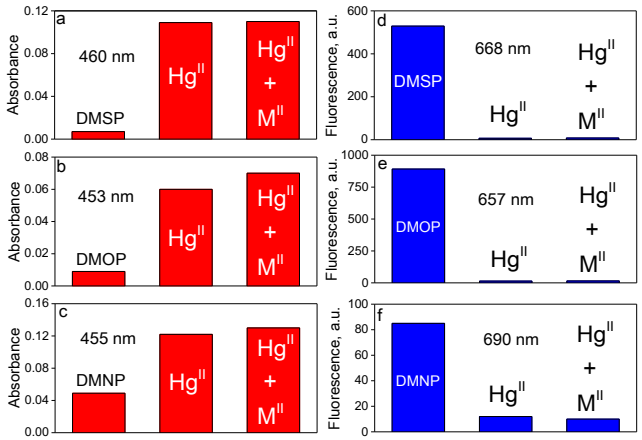

Fig. 12. Absorbance (a-c) and fluorescence (d-f) intensity of the 10-layer LS film of **DMSP** (a, d), **DMOP** (b, e) and **DMNP** (c, f) before and after immersion in 0.1 mM Hg^{2+} aqueous solution and in aqueous solution containing 1 mM of Cu^{2+}, Zn^{2+}, Cd^{2+}, Pb^{2+} and 0.1 mM Hg^{2+} perchlorates.

To demonstrate the key role of molecular organization in sensory properties of these LS films, a cast film of porphyrin **DMSP** was deposited onto a glass slide from a chloroform solution of this ligand. This film changes the colour in the presence of Hg^{2+}, Cu^{2+}, Zn^{2+}, Cd^{2+} and Pb^{2+} ions (Fig. S21) and slowly washes out from the solid surface.

We also prepared LS films transferring **TPP** and **TPyP** monolayers onto PVC slides under the same experimental conditions as was used to prepare **DMOP**, **DMSP** and **DMNP** sensors. UV–vis spectra of these films were remained unchanged after their exposure to 10^{-4} M aqueous solutions of mercury(II) perchlorate for 60 min (Fig. S24).

4. Conclusions

To prepare stable and sensitive ultra-thin porphyrin films responding to the binding of toxic metals, we have adapted the structural parameters of tetrapyrrolic molecules by tuning their hydrophilic-lipophilic balance, the size of substituents and introducing the donor heteroatoms at the periphery of the porphyrin macrocycle. To this end, XC_8H_{17}-functionalized (X = O, S, NH) 10,20-dimesitylporphyrin-5-ylphosphonate diesters **DMOP, DMSP** and **DMNP** were prepared according the synthetic approach developed by us previously. The target compounds were obtained in good yields after careful optimization of the nucleophilic substitution reactions.

These amphiphilic compounds form stable Langmuir monolayers at the air–water interface. In these floating films, porphyrin molecules display a slipped stack-of-card orientation, but their strong π-π stacking is prohibited by sterically demanding diethoxyphosphoryl and mesityl groups located at *meso*-positions of the macrocycle. The heteroatom substituent plays a key role in the molecular organization of these floating films due to its participation in intermolecular hydrogen bonding.

Sensing properties of the monolayers remarkably differ from those of their molecular precursors in the solution environment. The films are suitable for selective spectrophotometric detection of Hg^{2+} ions in aqueous environment because interfering Cu^{2+}, Zn^{2+}, Cd^{2+}, and Pb^{2+} ions are coordinated to the donor atoms at the periphery of the macrocycle.

Deposition of these floating films on the PVC surfaces by LS method affords multilayer films with a quite dense coverage of the solid support by sensing molecules. Both absorption and emission studies of these films have provided strong evidence in favor of very weak chromophore interactions. Interestingly, the heteroatom substituent has a significant effect on the surface pressure-assisted supramolecular assembly of porphyrins on the solid surfaces. However, in all ordered films, the receptor layers are accessible to mercury(II) ions.

Despite differences in molecular organization, all studied multilayer films can be used as solid-state dual-channel (absorption and emission) reusable Hg^{2+} sensors since only Hg^{2+} ions are coordinated to the tetrapyrrolic macrocycle, while other metals (Cu^{2+}, Zn^{2+}, Cd^{2+} and Pb^{2+}) are ligated to the peripheral donor sites if at all. The attenuation of the porphyrin association in the film makes the adsorption of Hg^{2+} ions easier and allows for their desorption under acidic conditions.

The instrumental optical response of these films can be obtained at Hg^{2+} concentrations above 10^{-8} M (2 ppb), which corresponds to the action level for Hg^{2+} ions in drinking water recommended by EPA. Moreover, these sensors can be used for the naked-eye colorimetric detection of the analyte in aqueous solutions in the presence of interfering Cu^{2+}, Zn^{2+}, Cd^{2+} and Pb^{2+} ions.

While LOD and selectivity of these sensory systems are comparable to the best previously reported solid-state sensors based on porphyrin derivatives (Table S1), they are prepared by using cost-efficient solid supports and minimal amounts of porphyrins. These sensors allow for simple miniaturization of sensory devices and can be used in field conditions. Their selectivity is determined by the porphyrin structure and is independent on the properties of the solid support, which is important in the analysis of environmental samples containing many unidentified interfering compounds.

ACKNOWLEDGEMENTS

This work was supported by the Centre National de la Recherche Scientifique (CNRS) and by the Russian Academy of Sciences (RAS), Russian Foundation for Basic Research (grants no. 17-53-16018 and 18-33-00339). This work was carried out in the framework of the International Associated French–Russian Laboratory of Macrocyclic Systems and Related Materials (LAMREM) of CNRS. Structural measurements were performed using equipment of CKP FMI IPCE RAS. The authors acknowledge Dr. Alexander E. Baranchikov and Dr. Shiryaev A. for technical support.

Appendix A. Supplementary data

Supplementary data to this article can be found online at https://doi.org/.

REFERENCES

[1] Eagles-Smith CA, Silbergeld EK, Basu N, Bustamante P, Diaz-Barriga F, Hopkins WA, Kidd KA, Nyland JF. Modulators of mercury risk to wildlife and humans in the context of rapid global change. Ambio 2018; 47(2): 170-197.

[2] Ghangrekar M, Chatterjee P. Water Pollutants Classification and Its Effects on Environment. In: Das R, editor. Carbon Nanotubes for Clean Water: Springer International Publishing; 2018. p. 11-26.

[3] Budnik LT, Casteleyn L. Mercury pollution in modern times and its socio-medical consequences. Sci Total Environ 2019; 654: 720-734.

[4] Mishra S, Bharagava RN, More N, Yadav A, Zainith S, Mani S, Chowdhary P. Heavy metal contamination: An alarming threat to environment and human health. Environmental biotechnology: For sustainable future. Singapore: Springer; 2019. p. 103-125.

[5] US EPA, Ground Water and Drinking Water, National Primary Drinking Water Regulations (NPDWR). https://www.epa.gov/ground-water-and-drinking-water/national-primary-drinking-water-regulations#Inorganic (accessed 03 July).

[6] Monti D, Venanzi M, Russo M, Bussetti G, Goletti C, Montalti M, Zaccheroni N, Prodi L, Rella R, Manera MG, Mancini G, Di Natale C, Paolesse R. Spontaneous deposition of amphiphilic porphyrin films on glass. New J Chem 2004; 28(9): 1123-1128.

[7] Wang L, Li H, Deng J, Cao D. Recent Advances in Porphyrin-Derived Sensors. Curr Org Chem 2013; 17(24): 3078-3091.

[8] Paolesse R, Nardis S, Monti D, Stefanelli M, Di Natale C. Porphyrinoids for Chemical Sensor Applications. Chem Rev 2017; 117(4): 2517-2583.

[9] Purrello R, Gurrieri S, Lauceri R. Porphyrin assemblies as chemical sensors. Coord Chem Rev 1999; 190-192: 683-706.

[10] Rakow NA, Suslick KS. A colorimetric sensor array for odour visualization. Nature 2000; 406(6797): 710-713.

[11] Itagaki Y, Deki K, Nakashima S-I, Sadaoka Y. Toxic gas detection using porphyrin dispersed polymer composites. Sens Actuators, B 2005; 108(1): 393-397.

[12] Tao S, Shi Z, Li G, Li P. Hierarchically Structured Nanocomposite Films as Highly Sensitive Chemosensory Materials for TNT Detection. ChemPhysChem 2006; 7(9): 1902-1905.

[13] Lee H, Hong K-I, Jang W-D. Design and applications of molecular probes containing porphyrin derivatives. Coord Chem Rev 2018; 354: 46-73.

[14] Di Natale C, Monti D, Paolesse R. Chemical sensitivity of porphyrin assemblies. Mater Today 2010; 13(7): 46-52.

[15] Drain CM, Hupp JT, Suslick KS, Wasielewski MR, Chen X. A perspective on four new porphyrin-based functional materials and devices. J Porphyrins Phthalocyanines 2002; 06(04): 243-258.

[16] Vandevyver M, Barraud A, Raudel T, Maillard P, Gianotti C. Structure of porphyrin multilayers obtained by the Langmuir Blodgett technique. J Colloid Interface Sci 1982; 85(2): 571-585.

[17] Czolk R, Reichert J, Ache HJ. An optical sensor for the detection of heavy metal ions. Sens Actuators, B 1992; 7(1): 540-543.

[18] Azim SA, El-Kemary MA, El-Daly SA, El-Daly HA, El-Khouly ME, Ebeid EM. Fluorescence quenching and complexation behaviour of tetraphenylporphyrin with some divalent metal ions. J Chem Soc, Faraday Trans 1996; 92(5): 747-751.

[19] Kilian K, Pyrzyńska K. Spectrophotometric study of Cd(II), Pb(II), Hg(II) and Zn(II) complexes with 5,10,15,20-tetrakis(4-carboxylphenyl)porphyrin. Talanta 2003; 60(4): 669-678.

[20] Valicsek Z, Horváth O. Application of the electronic spectra of porphyrins for analytical purposes: The effects of metal ions and structural distortions. Microchem J 2013; 107: 47-62.

[21] Chen Y, Wan L, Yu X, Li W, Bian Y, Jiang J. Rational Design and Synthesis for Versatile FRET Ratiometric Sensor for Hg^{2+} and Fe^{2+}: A Flexible 8-Hydroxyquinoline Benzoate Linked Bodipy-Porphyrin Dyad. Org Lett 2011; 13(21): 5774-5777.

[22] Marcelo GA, Pires SM, Faustino MAF, Simoes MM, Neves MGP, Santos HM, Capelo JL, Mota JP, Lodeiro C, Oliveira E. New dual colorimetric/fluorimetric probes for Hg^{2+} detection & extraction based on mesoporous SBA-16 nanoparticles containing porphyrin or rhodamine chromophores. Dyes Pigm 2019; 161: 427-437.

[23] Yang R, Li Ka, Wang K, Liu F, Li N, Zhao F. Cyclodextrin-porphyrin supramolecular sensitizer for mercury(II) ion. Anal Chim Acta 2002; 469(2): 285-293.

[24] Zhang Y, Xiang W, Yang R, Liu F, Li K. Highly selective sensing of lead ion based on α-, β-, γ-, and δ-tetrakis(3,5-dibromo-2-hydroxylphenyl)porphyrin/β-CD inclusion complex. J Photochem Photobiol, A 2005; 173(3): 264-270.

[25] Huang W-B, Gu W, Huang H-X, Wang J-B, Shen W-X, Lv Y-Y, Shen J. A porphyrin-based fluorescent probe for optical detection of toxic Cd^{2+} ion in aqueous solution and living cells. Dyes Pigm 2017; 143: 427-435.

[26] Weng Y-Q, Yue F, Zhong Y-R, Ye B-H. A Copper(II) Ion-Selective On–Off-Type Fluoroionophore Based on Zinc Porphyrin–Dipyridylamino. Inorg Chem 2007; 46(19): 7749-7755.

[27] Li C-Y, Zhang X-B, Qiao L, Zhao Y, He C-M, Huan S-Y, Lu L-M, Jian L-X, Shen G-L, Yu R-Q. Naphthalimide–Porphyrin Hybrid Based Ratiometric Bioimaging Probe for Hg^{2+}: Well-Resolved Emission Spectra and Unique Specificity. Anal Chem 2009; 81(24): 9993-10001.

[28] Choi JK, Sargsyan G, Olive AM, Balaz M. Highly Sensitive and Selective Spectroscopic Detection of Mercury(II) in Water by Using Pyridylporphyrin–DNA Conjugates. Chem - Eur J 2013; 19(7): 2515-2522.

[29] He X, Yang D, Chen H, Zheng W, Li H. A highly sensitive and reversible chemosensor for Hg^{2+} detection based on porphyrin-thymine conjugates. J Mol Recognit 2015; 28(5): 293-298.

[30] Han Z-X, Luo H-Y, Zhang X-B, Kong R-M, Shen G-L, Yu R-Q. A ratiometric chemosensor for fluorescent determination of Hg^{2+} based on a new porphyrin-quinoline dyad. Spectrochim Acta, Part A 2009; 72(5): 1084-1088.

[31] Liu X, Qi C, Bing T, Cheng X, Shangguan D. Highly Selective Phthalocyanine–Thymine Conjugate Sensor for Hg^{2+} Based on Target Induced Aggregation. Anal Chem 2009; 81(9): 3699-3704.

[32] Guo Q, Zeng Q, Zhang X, Zhou X. Highly sensitive detection of mercury (II) in aqueous media by tetraphenylporphyrin with a metal ion receptor. Supramol Chem 2014; 26(10-12): 836-842.

[33] Delmarre D, Méallet R, Bied-Charreton C, Pansu RB. Heavy metal ions detection in solution, in sol–gel and with grafted porphyrin monolayers. J Photochem Photobiol, A 1999; 124(1): 23-28.

[34] Plaschke M, Czolk R, Ache HJ. Fluorimetric determination of mercury with a water-soluble porphyrin and porphyrin-doped sol-gel films. Anal Chim Acta 1995; 304(1): 107-113.

[35] Guo L, Zhang W, Xie Z, Lin X, Chen G. An organically modified sol–gel membrane for detection of mercury ions by using 5,10,15,20-tetraphenylporphyrin as a fluorescence indicator. Sens Actuators, B 2006; 119(1): 209-214.

[36] Yari A, Abdoli HA. Sol–gel derived highly selective optical sensor for sensitive determination of the mercury(II) ion in solution. J Hazard Mater 2010; 178(1): 713-717.

[37] Magna G, Dinc Zor S, Catini A, Capuano R, Basoli F, Martinelli E, Paolesse R, Di Natale C. Surface arrangement dependent selectivity of porphyrins gas sensors. Sens Actuators, B 2017; 251: 524-532.

[38] Moura NMM, Nuñez C, Santos SM, Faustino MAF, Cavaleiro JAS, Neves MGPMS, Capelo JL, Lodeiro C. Functionalized Porphyrins as Red Fluorescent Probes for Metal Cations: Spectroscopic, MALDI-TOF Spectrometry, and Doped-Polymer Studies. ChemPlusChem 2013; 78(10): 1230-1243.

[39] Moura NMM, Núñez C, Santos SM, Faustino MAF, Cavaleiro JAS, Almeida Paz FA, Neves MGPMS, Capelo JL, Lodeiro C. A New 3,5-Bisporphyrinylpyridine Derivative as a Fluorescent Ratiometric Probe for Zinc Ions. Chem - Eur J 2014; 20(22): 6684-6692.

[40] Moura NMM, Núñez C, Faustino MAF, Cavaleiro JAS, Neves MGPMS, Capelo JL, Lodeiro C. Preparation and ion recognition features of porphyrin–chalcone type compounds as efficient red-fluorescent materials. J Mater Chem C 2014; 2(24): 4772-4783.

[41] Wang Y, Wu F. Amphiphilic acrylamide-based copolymer with porphyrin pendants for the highly selective detection of Hg^{2+} in aqueous solutions. Polymer 2015; 56: 223-228.

[42] Chan WH, Yang RH, Wang KM. Development of a mercury ion-selective optical sensor based on fluorescence quenching of 5,10,15,20-tetraphenylporphyrin. Anal Chim Acta 2001; 444(2): 261-269.

[43] Yang Y, Jiang J, Shen G, Yu R. An optical sensor for mercury ion based on the fluorescence quenching of tetra(p-dimethylaminophenyl)porphyrin. Anal Chim Acta 2009; 636(1): 83-88.

[44] Shamsipur M, Sadeghi M, Beyzavi MH, Sharghi H. Development of a novel fluorimetric bulk optode membrane based on meso-tetrakis(2-hydroxynaphthyl) porphyrin (MTHNP) for highly

sensitive and selective monitoring of trace amounts of Hg^{2+} ions. Mater Sci Eng, C 2015; 48: 424-433.

[45] Zhang X-B, Guo C-C, Li Z-Z, Shen G-L, Yu R-Q. An Optical Fiber Chemical Sensor for Mercury Ions Based on a Porphyrin Dimer. Anal Chem 2002; 74(4): 821-825.

[46] Cho Y, Lee SS, Jung JH. Recyclable fluorimetric and colorimetric mercury-specific sensor using porphyrin-functionalized Au@SiO2 core/shell nanoparticles. Analyst 2010; 135(7): 1551-1555.

[47] Liu B-W, Chen Y, Song B-E, Liu Y. Amphiphilic porphyrin assembly as a highly selective chemosensor for organic mercury in water. Chem Commun 2011; 47(15): 4418-4420.

[48] Sun L, Li Y, Sun M, Wang H, Xu S, Zhang C, Yang Q. Porphyrin-functionalized Fe3O4@SiO2 core/shell magnetic colorimetric material for detection, adsorption and removal of Hg^{2+} in aqueous solution. New J Chem 2011; 35(11): 2697-2704.

[49] Hu Y, Meng L, Lu Q. "Fastening" Porphyrin in Highly Cross-Linked Polyphosphazene Hybrid Nanoparticles: Powerful Red Fluorescent Probe for Detecting Mercury Ion. Langmuir 2014; 30(15): 4458-4464.

[50] Liu X, Liu X, Tao M, Zhang W. A highly selective and sensitive recyclable colorimetric Hg^{2+} sensor based on the porphyrin-functionalized polyacrylonitrile fiber. J Mater Chem A 2015; 3(25): 13254-13262.

[51] Zare-Dorabei R, Rahimi R, Koohi A, Zargari S. Preparation and characterization of a novel tetrakis(4-hydroxyphenyl)porphyrin–graphene oxide nanocomposite and application in an optical sensor and determination of mercury ions. RSC Adv 2015; 5(113): 93310-93317.

[52] Yang J, Wang Z, Li Y, Zhuang Q, Zhao W, Gu J. Porphyrinic MOFs for reversible fluorescent and colorimetric sensing of mercury(ii) ions in aqueous phase. RSC Adv 2016; 6(74): 69807-69814.

[53] Balaji T, Sasidharan M, Matsunaga H. Optical sensor for the visual detection of mercury using mesoporous silica anchoring porphyrin moiety. Analyst 2005; 130(8): 1162-1167.

[54] Dolci LS, Marzocchi E, Montalti M, Prodi L, Monti D, Di Natale C, D'Amico A, Paolesse R. Amphiphilic porphyrin film on glass as a simple and selective solid-state chemosensor for aqueous Hg^{2+}. Biosens Bioelectron 2006; 22(3): 399-404.

[55] Caselli M. Porphyrin-based electrostatically self-assembled multilayers as fluorescent probes for mercury(ii) ions: a study of the adsorption kinetics of metal ions on ultrathin films for sensing applications. RSC Adv 2015; 5(2): 1350-1358.

[56] Fang Z, Pu K-Y, Liu B. Asymmetric Fluorescence Quenching of Dual-Emissive Porphyrin-Containing Conjugated Polyelectrolytes for Naked-Eye Mercury Ion Detection. Macromolecules (Washington, DC, U S) 2008; 41(22): 8380-8387.

[57] Fang Z, Liu B. A cationic porphyrin-based self-assembled film for mercury ion detection. Tetrahedron Lett 2008; 49(14): 2311-2315.

[58] Ulman A. An Introduction of Ultrathin Organic Films From Langmuir-Blodgett to Self-Assembly; Academic Press: New York, 1991. New York: Academic Press:, 1991.

[59] Ulman A. Formation and Structure of Self-Assembled Monolayers. Chem Rev 1996; 96(4): 1533-1554.

[60] Petty MC. Langmuir-Blodgett film: an Introduction. Cambridge: Cambridge University Press, 1996.

[61] Petty MC. Film Deposition. In: Roberts G, editor. Langmuir-Blodgett Films: Springer US; 1990. p. 93-132.

[62] Zasadzinski JA, Viswanathan R, Madsen L, Garnaes J, Schwartz DK. Langmuir-Blodgett films. Science 1994; 263(5154): 1726.

[63] Zhang Y, Chen P, Ma Y, He S, Liu M. Acidification and assembly of porphyrin at an interface: counterion matching, selectivity, and supramolecular chirality. ACS Appl Mater Interfaces 2009; 1(9): 2036-2043.

[64] Chou H, Chen C-T, Stork KF, Bohn PW, Suslick KS. Langmuir-Blodgett Films of Amphiphilic Push-Pull Porphyrins. J Phys Chem 1994; 98(2): 383-385.

[65] Grieve MB, Hudson AJ, Richardson T, Johnstone RAW, Sobral AJFN, Rocha Gonsalves AMdA. An investigation of the optical properties of tetraphenylporphyrin derivatives in Langmuir and Langmuir-Blodgett films. Thin Solid Films 1994; 243(1): 581-586.

[66] Martı´in MaT, Prieto I, Muñoz E, Camacho L, Avila JL. A Revised Study on Formation at Air-Water Interface of Metallotetraphenylporphyrin Monolayers. J Colloid Interface Sci 1995; 175(1): 83-87.

[67] Liu H-G, Feng X-S, Xue Q-B, Wang L, Yang K-Z. Central metal effect on the organization of porphyrin LB films. Thin Solid Films 1999; 340(1): 265-270.

[68] Ni Y, Puthenkovilakom RR, Huo Q. Synthesis and Supramolecular Self-Assembly Study of a Novel Porphyrin Molecule in Langmuir and Langmuir−Blodgett Films. Langmuir 2004; 20(7): 2765-2771.

[69] Yao M, Iwamura Y, Inoue H, Yoshioka N. Amphiphilic meso-Disubstituted Porphyrins: Synthesis and the Effect of the Hydrophilic Group on Absorption Spectra at the Air−Water Interface. Langmuir 2005; 21(2): 595-601.

[70] Sun P, Jose DA, Shukla AD, Shukla JJ, Das A, Rathman JF, Ghosh P. A Comparative Langmuir–Blodgett Study on a Set of Covalently Linked Porphyrin-Based Amphiphiles: A Detailed Atomic Force Microscopic Study. Langmuir 2005; 21(8): 3413-3423.

[71] Valli L, Casilli S, Giotta L, Pignataro B, Conoci S, Borovkov VV, Inoue Y, Sortino S. Ethane-Bridged Zinc Porphyrin Dimers in Langmuir–Shäfer Thin Films: Structural and Spectroscopic Properties. J Phys Chem B 2006; 110(10): 4691-4698.

[72] Giancane G, Borovkov V, Inoue Y, Valli L. Conformational switching in bis(zinc porphyrin) Langmuir–Schaefer film as an effective tool for selectively sensing aromatic amines. J Colloid Interface Sci 2012; 385(1): 282-284.

[73] Auwärter W, Écija D, Klappenberger F, Barth JV. Porphyrins at interfaces. Nat Chem 2015; 7(2): 105-120.

[74] Ermakova EV, Meshkov IN, Yu. Enakieva Y, Zvyagina AI, Ezhov AA, Mikhaylov AA, Gorbunova YG, Chernyshev VV, Kalinina MA, Arslanov VV. Effect of metalation-demetalation reactions on the assembly and properties of 2D supramolecular arrays of tetrapyridylporphyrin and its Zn(II)-complex. Surf Sci 2017; 660: 39-46.

[75] Kroon JM, Sudhoelter EJR, Schenning APHJ, Nolte RJM. Self-Organization of Amphiphilic Porphyrins at the Air-Water Interface. Langmuir 1995; 11(1): 214-220.

[76] Honeybourne CL, Barrell KJ. Synthesis, spectroscopic characterization and thin film deposition of three novel amphiphilic porphyrins. J Porphyrins Phthalocyanines 1999; 3(6-7): 569-584.

[77] Okada S, Segawa H. Substituent-Control Exciton in J-Aggregates of Protonated Water-Insoluble Porphyrins. J Am Chem Soc 2003; 125(9): 2792-2796.

[78] Liu H-G, Feng X-S, Zhang L-J, Ji G-L, Qian D-J, Lee Y-I, Yang K-Z. Influences of hydrophilic and hydrophobic substituents on the organization of supramolecular assemblies of porphyrin derivatives formed at the air/water interface. Mater Sci Eng, C 2003; 23(5): 585-592.

[79] Dunbar ADF, Richardson TH, McNaughton AJ, Hutchinson J, Hunter CA. Investigation of Free Base, Mg, Sn, and Zn Substituted Porphyrin LB Films as Gas Sensors for Organic Analytes. J Phys Chem B 2006; 110(33): 16646-16651.

[80] Hosomizu K, Oodoi M, Umeyama T, Matano Y, Yoshida K, Isoda S, Isosomppi M, Tkachenko NV, Lemmetyinen H, Imahori H. Substituent Effects of Porphyrins on Structures and Photophysical Properties of Amphiphilic Porphyrin Aggregates. J Phys Chem B 2008; 112(51): 16517-16524.

[81] Bussetti G, Corradini C, Goletti C, Chiaradia P, Russo M, Paolesse R, Di Natale C, D'Amico A, Valli L. Optical anisotropy and gas sensing properties of ordered porphyrin films. Phys Status Solidi B 2005; 242(13): 2714-2719.

[82] Pedrosa JMa, Dooling CM, Richardson TH, Hyde RK, Hunter CA, Martín MaT, Camacho L. The optical gas-sensing properties of an asymmetrically substituted porphyrin. J Mater Chem 2002; 12(9): 2659-2664.

[83] Stich MIJ, Fischer LH, Wolfbeis OS. Multiple fluorescent chemical sensing and imaging. Chem Soc Rev 2010; 39(8): 3102-3114.

[84] Bussetti G, Violante A, Yivlialin R, Cirilli S, Bonanni B, Chiaradia P, Goletti C, Tortora L, Paolesse R, Martinelli E, D'Amico A, Di Natale C, Giancane G, Valli L. Site-Sensitive Gas Sensing and Analyte Discrimination in Langmuir–Blodgett Porphyrin Films. J Phys Chem C 2011; 115(16): 8189-8194.

[85] Giancane G, Valli L. State of art in porphyrin Langmuir–Blodgett films as chemical sensors. Adv Colloid Interface Sci 2012; 171-172: 17-35.

[86] Yang W, Xu J, Mao Y, Yang Y, Jiang Y. Detection of Volatile Organic Compounds Using Langmuir-Blodgett Films of Zinc-Porphyrin and Zinc-Phthalocyanine. Synth React Inorg, Met-Org, Nano-Met Chem 2016; 46(5): 735-740.

[87] Giancane G, Borovkov V, Inoue Y, Conoci S, Valli L. Syn–anti conformation switching of a bis-porphyrin derivative at the air–water interface and in the solid state as an effective tool for chemical sensing. Soft Matter 2013; 9(7).

[88] Taneja P, Khandagale SB, Manjuladevi V, Gupta RK, Kumar D, G upta KK. Heavy Metal Ion Sensing Using Ultrathin Langmuir–Schaefer Film of Tetraphenylporphyrin Molecule. IEEE Sens J 2020; 20(7): 3442-3451.

[89] Bettini S, Pagano R, Valli L, Giancane G. Spectroscopic Investigation of the Selective Interaction of Mercuric and Cupric Ions with a Porphyrin Active Layer. J Phys Chem C 2014; 118(23): 12384-12390.

[90] Pavinatto FJ, Gameiro AF, Hidalgo AA, Dinelli LR, Romualdo LL, Batista AA, Neto NMB, Ferreira M, Oliveira ON. Langmuir and Langmuir–Blodgett (LB) films of tetrapyridyl metalloporphyrins. Appl Surf Sci 2008; 254(18): 5946-5952.

[91] de Miguel G, Hosomizu K, Umeyama T, Matano Y, Imahori H, Pérez-Morales M, Martín-Romero MT, Camacho L. J-aggregation of a sulfonated amphiphilic porphyrin at the air–water interface as a function of pH. J Colloid Interface Sci 2011; 356(2): 775-782.

[92] Yu W, Li Z, Wang T, Liu M. Aggregation and supramolecular chirality of achiral amphiphilic metalloporphyrins. J Colloid Interface Sci 2008; 326(2): 460-464.

[93] Ermakova EV, Enakieva YY, Nefedov SE, Arslanov VV, Gorbunova YG, Tsivadze AY, Stern C, Bessmertnykh-Lemeune A. Synthesis of (trans-A2)BC-Type Porphyrins with Acceptor Diethoxyphosphoryl and Various Donor Groups and their Assembling in the Solid State and at Interfaces. Eur J Org Chem 2019; 2019(20): 3146-3162.

[94] Spartan 14.V1.1.4., Wavefunction, Inc., 18401, Von Karman Avenue, Suite 370, Irvine CA 92612 USA.

[95] Wen B, Xue J, Zhou X, Wu Q, Nie J, Xu J, Du B. Highly selective and sensitive detection of Pb^{2+} in aqueous solution using tetra (4-pyridyl) porphyrin-functionalized Thermosensitive ionic microgels. ACS Appl Mater Interfaces 2018; 10(30): 25706-25716.

[96] Huang TC, Toraya H, Blanton TN, Wu Y. X-ray powder diffraction analysis of silver behenate, a possible low-angle diffraction standard. J Appl Crystallogr 1993; 26(2): 180-184.

[97] Gouterman M. Study of the Effects of Substitution on the Absorption Spectra of Porphin. J Chem Phys 1959; 30(5): 1139-1161.

[98] Gouterman MJ. Optical Spectra and Electronic Structure of Porphyrins and Related Rings. In: D'olpin D, editor. The Porphyrins. 3rd ed. New York: Academic Press; 1978. p. 1-165.

[99] Horváth O, Huszánk R, Valicsek Z, Lendvay G. Photophysics and photochemistry of kinetically labile, water-soluble porphyrin complexes. Coord Chem Rev 2006; 250(13): 1792-1803.

[100] Valicsek Z, Lendvay G, Horváth O. Equilibrium, Photophysical, Photochemical, and Quantum Chemical Examination of Anionic Mercury(II) Mono- and Bisporphyrins. J Phys Chem B 2008; 112(46): 14509-14524.

[101] Chen P, Ma X, Duan P, Liu M. Chirality Amplification of Porphyrin Assemblies Exclusively Constructed from Achiral Porphyrin Derivatives. ChemPhysChem 2006; 7(11): 2419-2423.

[102] Giancane G, Guascito MR, Malitesta C, Mazzotta E, Picca RA, Valli L. QCM sensors for aqueous phenols based on active layers constituted by tetrapyrrolic macrocycle Langmuir films. J Porphyrins Phthalocyanines 2009; 13(11): 1129-1139.

[103] M. Kasha M, H. R. Rawls HR, El-Bayoumi MA. The exciton model in molecular spectroscopy. Pure Appl Chem 1965; 11(3-4): 371-392.

[104] de Miguel G, Hosomizu K, Umeyama T, Matano Y, Imahori H, Martín-Romero MT, Camacho L. Tunable Soret-Band Splitting of an Amphiphilic Porphyrin by Surface Pressure. ChemPhysChem 2008; 9(11): 1511-1513.

[105] Schick GA, Schreiman IC, Wagner RW, Lindsey JS, Bocian DF. Spectroscopic characterization of porphyrin monolayer assemblies. J Am Chem Soc 1989; 111(4): 1344-1350.

[106] Azumi R, Matsumoto M, Kawabata Y, Kuroda S, Sugi M, King LG, Crossley MJ. Orientation change of porphyrin in Langmuir-Blodgett films caused by a trigger molecule. J Phys Chem 1993; 97(49): 12862-12869.

[107] Qiu Y, Chen P, Liu M. Interfacial Assembly of an Achiral Zinc Phthalocyanine at the Air/Water Interface: A Surface Pressure Dependent Aggregation and Supramolecular Chirality. Langmuir 2008; 24(14): 7200-7207.

[108] Qian D-J, Nakamura C, Miyake J. Multiporphyrin Array from Interfacial Metal-Mediated Assembly and Its Langmuir–Blodgett Films. Langmuir 2000; 16(24): 9615-9619.

[109] Giovannetti R, Bartocci V. Kinetic and equilibrium studies on mercury(II)-coproporphyrin-I. Metal ion exchange reaction with cobalt(II) and application to determination of trace mercury(II). Talanta 1998; 46(5): 977-984.

[110] Horváth O, Valicsek Z, Vogler A. Unique photoreactivity of mercury(II) 5,10,15,20-tetrakis(4-sulfonatophenyl)porphyrin. Inorg Chem Commun 2004; 7(7): 854-857.

[111] Dooling CM, Worsfold O, Richardson TH, Tregonning R, Vysotsky MO, Hunter CA, Kato K, Shinbo K, Kaneko F. Fast, reversible optical sensing of NO_2 using 5,10,15,20-tetrakis[3,4-bis(2-ethylhexyloxy)phenyl]-21H,23H-porphine assemblies. J Mater Chem 2001; 11(2): 392-398.